April 2010

Electrochemical Characterization and Water Balance of a PEM Fuel Cell

Andrew William Emerson
Worcester Polytechnic Institute

Laura Elizabeth Moreno
Worcester Polytechnic Institute

Project Number: FR50

Electrochemical Characterization and Water Balance of a PEM Fuel Cell

A Major Qualifying Project Report
submitted to the faculty of
WORCESTER POLYTECHNIC INSTITUTE
in partial fulfillment of the requirements for the
Degree of Bachelor of Science
by

_____
Andrew Emerson

_____
Laura Montville

Date: April 29, 2010

_____
Professor Ravindra Datta, Advisor (WPI)

_____
Professor François Lapicque, Co-Advisor (ENSIC, France)

Table of Contents

Table of Figures

Table of Tables

Acknowledgements

We would like to thank the following persons in no particular order for their invaluable contributions to our project.

Botao Huang

Caroline Bonnet

Francois Lapicque

The LRGP Group

Professor Ravindra Datta

Professor Terri Camesano

Abstract

This project was completed at ENSIC in Nancy, France. The water content of a fuel cell is crucial to performance, as are resistance values. This project studied a polymer electrolyte membrane (PEM) fuel cell under varied feed flow rates and hydrogen concentrations, while imposing dynamic current cycle between 0.12 A/cm^2 and 0.36 A/cm^2. Fuel cell performance was analyzed through the water balance and Galvano Electrochemical Impedance Spectroscopy. Results showed that the charge transfer resistance decreases as current density increases; lower concentrations of hydrogen feed gas result in higher anode resistances but do not affect cathode resistance; net water flow is from the cathode to the anode; 50% and 100% hydrogen feed cause flooding at the anode and cathode unless the stoichiometric ratio is raised; lower hydrogen concentrations reduce flooding; and the two theoretical models accurately represent the collected data.

Executive Summary

The objective of this project was to determine how various operating conditions affect the water content and resistances of a polymer electrolyte membrane (PEM) fuel cell. The experiments were completed in Nancy, France at Ecole Nationale Supérieure des Industries Chimiques (ENSIC).

The concentration of hydrogen being fed to the anode was varied between 10%, 20%, 50%, and 100% in nitrogen, and the stoichiometric ratio of hydrogen varied between 1.5, 3, and 7.5. A polarization curve was obtained for approximately one hour after reaching steady state, while applying a current density of 0.12, 0.24, or 0.36 A/cm^2. Over this period, water was collected at the exit of the anode and the cathode. The mass of water collected was then used to determine the water content in the fuel cell through the water transport coefficient and the water ratio.

After each polarization curve was obtained, Galvano Electrochemical Impedance Spectroscopy tests were run. They were conducted over a frequency range from 10 kHz to 100 mHz, at the same current density and feed gas conditions as the prior polarization experiment. The results from the impedance spectrum were fit to a theoretical model to determine the charge transfer resistance, diffusion resistance, and exchange current density of the fuel cell.

The following are the results for varied stoichiometric hydrogen feed. The cathode and anode charge transfer resistances were found to decrease with increasing current density and increase with increasing stoichiometric ratio. The cathode diffusion resistance decreased with increasing flow rates of hydrogen as well as increasing current density. In the case of pure hydrogen, the anode diffusion resistance was assumed to be zero as the diffusivity of hydrogen is very large. The water transport coefficient was positive for all flow rates and current densities, and with increasing flow rates the water transport coefficient increased. Flooding in the anode

occurred at the stoichiometric conditions of 1.5 and 3 but at 7.5 the anode was dry. Flooding in the cathode occurred at low current densities with stoichiometric conditions 1.5 and 3 but not with 7.5. At high current densities no flooding occurred.

When varying the concentration of hydrogen diluted with nitrogen, the cathode and anode charge transfer resistances were found to decrease with increasing current densities. The cathode resistance is much larger than the anode resistance and does not change with varying concentrations of hydrogen. The anode resistance varied proportionally with the hydrogen concentration. The anode and cathode diffusion resistance acted very similarly to the charge transfer resistance – decreasing with increasing current density. Again the cathode resistance did not change with the varying hydrogen concentration, while the anode resistance did change. The water transport coefficient was positive in all cases of hydrogen dilution. Flooding in the anode occurred in high concentrations of hydrogen (50% or higher). Flooding in the cathode occurred only at low current densities for 100% and 50% hydrogen.

The exchange current density of the anode was found to remain nearly constant with changing stoichiometric flow rates, but changed proportionally with the concentration and partial pressure of hydrogen. The cell output voltage was found to decrease with increasing current density as well as proportionally decrease with decreasing concentrations of hydrogen.

In conclusion, the theoretical models used in this project accurately predicted the collected data for both voltage and charge transfer resistance, and the water content of a fuel cell can be adjusted using various concentrations and stoichiometric ratios of hydrogen in the feed stream.

Notation

α: Water transport coefficient

α_a^*: Anode water transport coefficient

α_c^*: Cathode water transport coefficient

λ: Stoichiometric coefficient

σ_{EL}: Conductivity

τ_d: Diffusion time constant

τ_{da}: Time constant anode

τ_{dc}: Time constant in seconds for cathode

ω: Frequency

μ_f: Fuel utilization coefficient

ΔG_f: Change in Gibbs free energy of formation

$\Delta \bar{h}_f$: Change in enthalpy of formation

a: Activity

b_a: Tafel slope

C: Capacity of the electrical double layer

e: Charge on an electron

E: Fuel cell voltage

E^0: Electromotive force/open cell voltage

F: Faraday constant

F_x: Flow of material x

$\bar{g}_f$: Gibbs free energy of formation per mole

i_0: Exchange current density

i_{load}: Current load

j: Imaginary unit

L: Inductance (only at high frequency)

N: Avogadro's Number

n_a: Anode constant

n_c: Cathode constant

P: Partial pressure of gas

P^0: Standard pressure

Q_a: Pseudo capacity for anode

Q_c: Pseudo capacity for cathode

R: Static resistance

R_a: Electrolyte resistance

R_b: Activation resistance

$R_{ct,a}$: Charge transfer resistance for anode

$R_{ct,c}$: Charge transfer resistance for cathode

R_{da}: $R_{diff,A}$: diffusion resistance for anode

R_{dc}: $R_{diff,C}$: diffusion resistance for cathode

R_{diff}: Diffusion resistance

RH: Relative humidity

R_{ohm}: Ohmic Resistance

R_p: Overall cell resistance

r_{tc}: Ohmic resistance of charge transfer

y: Mole fraction (gas)

T: Temperature

υ_{Ae^-}: Stoichiometric coefficient of anode

υ_{Ce^-}: Stoichiometric coefficient of cathode

V_c: Measured voltage of a fuel cell

V_{load}: Voltage load

V_{OCV}: Potential of open circuit fuel cell

WR: Water ratio

Z_{FC}: Overall fuel cell impedance

Z_{RC}: Impedance in an RC circuit

Z_{RLC}: Impedance in an RLC circuit

Z_W: Warburg impedance

1.0 Introduction

The objective of this study was to analyze the charge transfer and diffusion resistances, the exchange current density, water transport coefficient, and water ratio of a fuel cell. The analysis of cell resistances is important so that optimal operating conditions may be established to minimize voltage loss in the cell. The analysis of resistances also is a key method in determining operational problems and malfunctions within the fuel cell. In a fuel cell, the water content is also very important. If there is not enough water, the fuel cell can dry out and crack, and if there is too much, the electrode pores can become blocked and flood. Both of these things can affect the operation of a fuel cell. This project will determine what experimental parameters will cause flooding or eliminate flooding.

A fuel cell is an electrochemical device that is used to create electricity. A battery is another electrochemical device, but the difference between the two is the source of fuel. A battery stores fuel inside, so eventually the fuel runs out and the battery is dead. A fuel cell, on the other hand, has external fuel sources that can be continuously fed to the cell (Nice and Strickland, 2010). The specific fuel can vary, and the types of fuel cells are named by the fuel they use.

Because fuel cells don't use fossil fuels, the only waste products from the reaction are heat and water. For this reason, and because they can be used in remote locations, fuel cells are being used in spacecraft, off-grid areas, and in public transportation.

2.0 Background

2.1 Fuel Cells

2.1.1 History

Despite fuel cells being called a new age energy source for the future by today's media, interest in fuel cells can be found as far back as 1838. In 1800, William Nicholson and Anthony Carlisle established the process of electrolysis to decompose water into hydrogen and oxygen (Cahan, Wieghaus and Schottel, 2006). In 1838, Christian Friedrich Schönbein published the theory of a fuel cell in one of the popular scientific magazines of the time – the Royal Society's Catalogue. Schönbein worked with the two schools of thought at the time as to the way fuel cells functioned. The Contact Theory hypothesized that physical contact between materials generated electricity. The Chemical Theory hypothesized that chemical reactions were what generated the electricity. In his publications, Schönbein hypothesized that the chemical theory was more accurate (Fuel Cell, 2010). William Robert Grove, through correspondence with Schönbein, built a prototype fuel cell. Grove arranged two platinum electrodes with one end of each immersed in a solution of sulfuric acid and the other ends in sealed containers of water with oxygen and hydrogen, respectively. Grove found that a constant current would flow between the plates, and the water level in each sealed container rose. He combined several of these plates in series to increase the produced charge. The "gas battery," as Grove titled his experiment, was the first fuel cell ever invented and gave birth to an avenue of electrochemistry which may hold the key to replacing fossil fuels in the future (Cahan, Wieghaus and Schottel, 2006).

In 1889, Ludwig Mond and Carl Langer constructed a hydrogen-oxygen fuel cell using perforated platinum electrodes which produced a current density of 6 amps per ft^2 (which corresponds to 0.0065 amperes per cm^2) with 0.73 volts. Then in 1893, Friedrich Wilhelm Ostwald experimentally determined the roles of the electrodes, oxidizing and reducing agents,

anions, electrolyte and cations in the fuel cell. Ostwald is considered one of the primary founders of physical chemistry. He was able to determine that the active area of the fuel cell was at the point of contact between the electrode, gas and electrolyte. Ostwald's research was expanded upon by Francis Thomas Bacon in the late 1930's. In 1939, Bacon built a fuel cell using nickel gauze electrodes which operated under pressures as high as 3000 psi in a solution of potassium hydroxide. World War II fueled research into all forms of energy sources and Bacon worked to develop a fuel cell for the British Royal Navy submarines; culminating in 1958 with Bacon's alkali cell which used a stack of 10 inch diameter electrodes for Britain's National Research Development Corporation. This resulted in a 5 kilowatt stationary fuel cell which was the first commercial fuel cell. It was used to power a welding machine. Bacon's design was purchased by Pratt & Whitney in the 1960s and was incorporated into the design of the fuel cells for the Apollo spacecraft fuel cells in order to supply electricity and drinking water to the spacecraft (Cahan, Wieghaus and Schottel, 2006).

At the same time as Bacon's work with the Royal Navy, Thomas Grub, working for General Electric, modified a fuel cell with a polystyrene ion-exchange membrane in 1955. Three years later, in 1958, Leonard Niedrach deposited platinum onto the polystyrene membrane allowing the catalyst increased proximity to the exchange for oxygen and hydrogen oxidation and reduction reactions. This fuel cell was named the Grubb-Niedrach fuel cell. General Electric developed this technology further in conjunction with NASA and McDonnell Aircraft; ultimately resulting in the use of fuel cells during Project Gemini which was the second human spaceflight by NASA. This fuel cell was based upon a Teflon solid electrolyte layer impregnated with acid. In 1959, Harry Ihrig built a 15 kilowatt fuel cell tractor as the first fuel cell powered vehicle for Allis-Chalmers using potassium hydroxide as the electrolyte and compressed

hydrogen and oxygen as reactants. In the mid 1960s General Motors designed an experimental fuel cell-powered van developed by Union Carbide (Fuel Cell, 2010), but the design proved to be inefficient and contained several design flaws (Barbir, 2005). The 1960s were a time of inexpensive fossil fuels and explosive growth and fuel cells experienced a lack of interest as the technology of the time could not produce sufficient energy density to power practical vehicles beyond prototypes. The mid 1970 oil shortages and environmental concerns reinvigorated the scientific communities' interest in fuel cells (Harper, 2008). Commercial fuel cells did not appear on a grand scale until 1989 when Perry Energy Systems of Perry Technologies Canada demonstrated a Polymer Electrolyte Membrane (PEM) fuel cell powered submarine. Then, in 1993, Ballard Power Systems demonstrated efficient fuel cell-powered buses and Energy Partners (a spinoff of Perry Energy Systems) developed the first passenger car to run on PEM fuel cells. 1993 proved to be a pivotal year in the development of commercial fuel cells. Car companies in the United States began to develop their own versions of fuel cell powered vehicles and by 2000 nearly every major car manufacturer had a prototype fuel cell-powered vehicle. Part of the interest in fuel cell vehicles came from fears of the infamous Y-2k bug and the impending fossil fuel crisis. After 2001 fuel cell company stocks fell as fears of millennium disasters dissipated. Despite the decline in stock prices in the early 2000s, the number of fuel-cell related patents in the United States and Japan has increased dramatically; indicating increased interest and involvement of the scientific and engineering community in the development of fuel cells (Barbir, 2005).

2003 became a momentous year for fuel cell development as the first public hydrogen filling station opened in Reykjavik, Iceland as a service terminal for the three hydrogen buses which operate in the city. As the energy density of fuel cells improves, fuel cells are being

implemented in more areas. In 2005 the first fuel cell motorcycle was released by Intelligent Energy. It is capable of traveling up to 50 miles per hour with a range of 100 miles. The Howaldtswerke-Deutsche Werf AG (HDW) out of Germany has developed a Class 212 fuel cell powered submarine. The submarine is powered by a PEM fuel cell and is capable of staying submerged for weeks without resurfacing (Harper, 2008).

2.1.2 Fuel Cell Basics

Hydrogen fuel cells operate in a fairly simple manner. In the same way that water can be electrolyzed into hydrogen and oxygen using a current of electricity, hydrogen and oxygen can combine to produce an electric current. The reaction is as follows, and works in a similar way to a combustion reaction, differing only in that fuel cells deliver electrical energy instead of heat energy:

$$2H_2 + O_2 \leftrightarrow 2H_2O \qquad (1)$$

A fuel cell is made out of electrodes and an electrolyte, commonly layered to give the maximum possible surface contact area, as seen in Figure 1 (Larminie and Dicks, 2003).

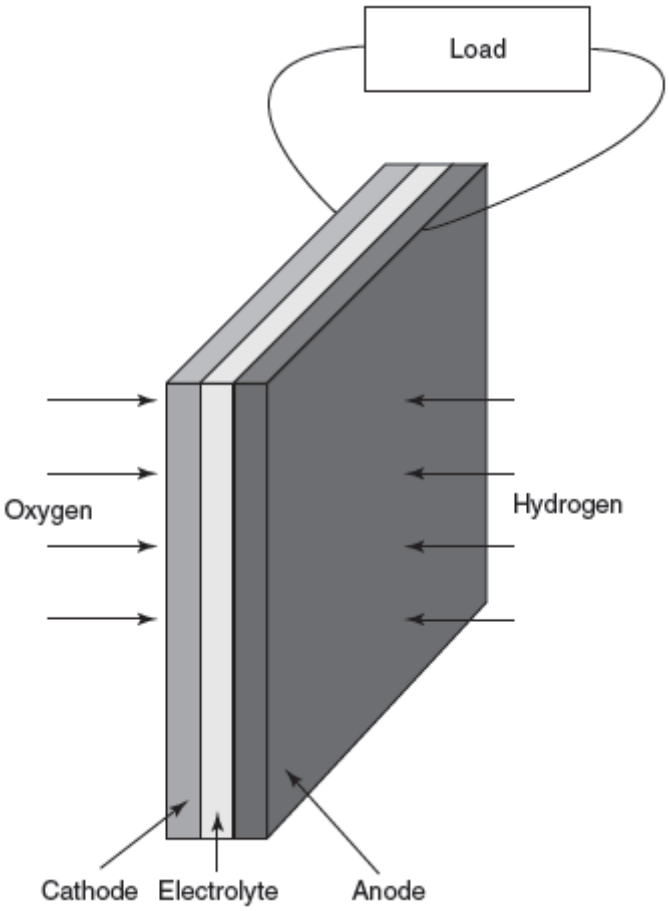

Figure 1: Fuel Cell

In an acid electrolyte cell, the following reaction takes place at the anode:

$$2H_2 \rightarrow 4H^+ + 4e^- \qquad (2)$$

and at the cathode:

$$O_2 + 4e^- + 4H^+ \rightarrow 2H_2O \qquad (3)$$

The hydrogen gas passing through the anode is ionized, splitting into protons (H^+ ions) and electrons and releasing energy. The protons pass through the electrolyte layer, while the electrons pass through an electrical circuit. When both have reached the cathode, they react with oxygen gas to form water (Larminie and Dicks, 2003).

The same overall reaction applies to alkaline electrolyte fuel cells, but instead of mobile H^+ ions, alkaline fuel cells have OH^- ions creating the current in the cell.

Anode:

$$2H_2 + 4OH^- \rightarrow 4H_2O + 4e^- \quad (4)$$

Cathode:

$$O_2 + 4e^- + H_2O \rightarrow 4OH^- \quad (5)$$

At the anode, the hydroxyl ions (OH^-) react with hydrogen to produce water. The water flows through the electrolyte and the electrons released from this reaction flow through the electrical circuit to the cathode, where they react with oxygen gas to form new hydroxyl ions. These in turn pass back through the electrolyte to react at the anode (Larminie and Dicks, 2003).

Although acid electrolyte fuel cells and alkaline electrolyte fuel cells are fully described here, there are many other types of fuel cells. Other types have different mobile ions, and may have different reactions taking place at the anode and cathode.

2.1.3 Types of Fuel Cells

Because various fuel cells use a range of electrolytes, they differ in operating temperature, catalyst, and chemical reaction, which makes them suitable for an assortment of applications. Here are some advantages and disadvantages of the most common types.

Polymer Electrolyte Membrane Fuel Cells

PEM fuel cells are relatively light and have a smaller volume than other types of fuel cells. Since they only use hydrogen, oxygen from air, and water to operate, they are used primarily for transportation and power in remote areas. They can start quickly, because the relatively low operating temperature of around 80°C does not require a large amount of warming up (U.S. Department of Energy, 2009), and PEM fuel cells last longer than other types of fuel cells because there are no corrosive fuels or high temperatures. However, they are more

expensive because a catalyst, often platinum, is required to separate the electrons and protons of the hydrogen gas, and as will be discussed in the Literature Review section, the catalyst can be poisoned by carbon monoxide traces in the hydrogen fuel gas. There is also a storage problem because hydrogen has such a low density. A vehicle run by pure hydrogen needs to refuel more often than one powered by gasoline.

Direct Methanol Fuel Cells

Whereas most fuel cells are powered by hydrogen, DMFCs are powered by feeding pure methanol to the anode. It is easier to store and transport methanol than hydrogen, because of its higher density and its liquid state. It can be supplied to users in a similar way to gasoline. However, the technology is relatively new, so it is 3-4 years behind other types of fuel cells in development (U.S. Department of Energy, 2009).

Alkaline Fuel Cells

AFCs use a potassium hydroxide solution as the electrolyte and can operate at temperatures between 23°C and 70°C. The chemical reaction in the cell occurs at a high rate, which gives AFCs a high performance, and the efficiency of these fuel cells used in space has reached 60%. Although AFCs were the first type of fuel cell widely used in the U.S. space program to produce electricity and water (U.S. Department of Energy, 2009), there is a problem with cost. They are easily poisoned by carbon dioxide, which reduces the life of the fuel cells and leads to expensive purification requirements for the hydrogen and the oxygen fuels.

Phosphoric Acid Fuel Cells

PAFCs, usually used in stationary power generation, use liquid phosphoric acid as an electrolyte. They are 85% efficient when generating electricity and heat together, but only 37-42% efficient when only producing electricity (U.S. Department of Energy, 2009). They aren't as easily poisoned by impurities in the hydrogen gas as PEM fuel cells are, but they are less

powerful so they have to be made much larger and heavier to produce comparable power. Lastly, the platinum catalyst also increases the cost of PAFCs.

Molten Carbonate Fuel Cells

MCFCs, which are used for electrical utility and military applications, have an electrolyte made of a blend of molten carbonate salts. They have a high efficiency of almost 60%, which increases to almost 85% when the waste heat is recycled. Because of a high operating temperature (650°C), non-precious metals can be used as catalysts. The catalysts and efficiency combined reduce the cost compared to other types of fuel cells. However, the high temperature and corrosive electrolyte cause the fuel cell to erode rapidly, and therefore parts require frequent replacement (U.S. Department of Energy, 2009).

Solid Oxide Fuel Cells

SOFCs have an electrolyte made out of a solid, non-porous ceramic compound, and like MCFCs, operate at a very high temperature (1000°C). Because of the similarly high operating temperatures, many of the advantages and disadvantages are also the same. SOFCs are 50-60% efficient, and 80-85% efficient when the heat is captured, and don't require a precious metal catalyst. The high temperature requires extra protection to reduce heat loss and protect personnel, and once again reduces the durability of the fuel cell (U.S. Department of Energy, 2009).

2.2 PEM Fuel Cell

2.2.1 Open Circuit Voltage

While the electrical power and energy output of a fuel cell can be easily determined by the equations $Power = VI$ and $Energy = VIt$, determining the chemical input and output involves more complex equations. One must look closely at the Gibbs free energy, which is the energy available to do external work. The external work in the case of a fuel cell is the movement of the electrons around the electrical circuit.

The energy released by a fuel cell can be determined by the Gibbs free energy of formation, ΔG_f, which is the difference between the Gibbs free energy of the products and the Gibbs free energy of the reactants. When considering the basic reaction for a fuel cell,

$$\mathrm{H_2} + \frac{1}{2}\mathrm{O_2} \rightarrow \mathrm{H_2O} \quad (6)$$

the Gibbs free energy on a "per mole" basis ($\Delta \bar{g}_f$) is

$$\Delta \bar{g}_f = \left(\bar{g}_f\right)_{H_2O} - \left(\bar{g}_f\right)_{H_2} - \frac{1}{2}(\bar{g}_f)_{O_2} \quad (7)$$

The Gibbs free energy of formation changes with temperature and the state of the water product, and these values can be found in literature. If a fuel cell is considered to be completely reversible, that is, all of the Gibbs free energy is converted to electrical energy, the reversible open circuit voltage can be calculated. Referring to the overall reaction that is occurring in a fuel cell, two electrons will pass through the circuit for every molecule of hydrogen that is converted to water. Therefore, if *N* is Avogadro's number (the number of molecules in a mole), *F* is the Faraday constant (the charge on one mole of electrons), and *–e* is the charge on one electron, the charge flowing through the fuel cell can be represented by:

$$-2Ne = -2F \quad (8)$$

The electrical work done by the fuel cell can then be determined, if *V* is the voltage of the fuel cell:

$$\text{Electrical work done} = \text{charge} \times \text{voltage} = -2FV \quad (9)$$

As stated, assuming the fuel cell to be reversible, this will be equal to the Gibbs free energy released. The electromotive force (EMF) or the reversible open circuit voltage (OCV) of the fuel cell is then:

$$V^0 = \frac{-\Delta \bar{g}_f{}^0}{2F} \quad (10)$$

2.2.2 Efficiency

In reality, fuel cells are not completely reversible, and therefore it is impossible to have an efficiency of 100%. The change in enthalpy of formation, $\Delta\bar{h}_f$, is the heat that is produced by burning the fuel, and can be compared to the Gibbs free energy, which is the electrical energy produced, to determine a maximum efficiency (Larminie and Dicks, 2003).

$$\text{maximum efficiency possible} = \frac{\Delta\bar{g}_f}{\Delta\bar{h}_f} \times 100\% \quad (11)$$

Because the Gibbs free energy varies with temperature, the efficiency of a fuel cell will also vary with temperature. A graph of maximum efficiency versus operating temperature can be seen in Figure 2 (Larminie and Dicks, 2003).

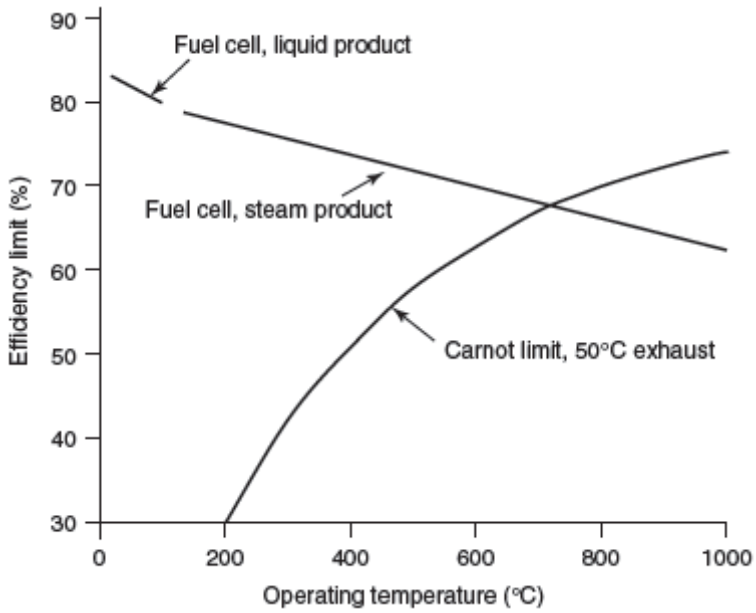

Figure 2: Efficiency vs. Operating Temperature

When calculating efficiency, there are two possible values of $\Delta\bar{h}_f$ to use. One comes from the burning of hydrogen gas to produce steam, which has a $\Delta\bar{h}_f$ of -241.83 kJ/mol. The second comes from the same reaction with the product being condensed to liquid, with a $\Delta\bar{h}_f$ of -285.84 kJ/mol. The lower heating value and higher heating value (respectively) should be specified when efficiency values are discussed.

For a 100% efficient fuel cell, the EMF would be 1.48 V if using the higher heating value in the EMF equation, and 1.25 if using the lower heating value. Therefore, the efficiency of a cell with a measured voltage V_c can be calculated from the equation:

$$\text{efficiency} = \frac{V_c}{1.48} * 100\% \quad (12)$$

(replacing the 1.48 with 1.25 if referring to the LHV) (Larminie and Dicks, 2003). Even more accuracy can be obtained by incorporating a fuel utilization coefficient, μ_f, into the equation.

$$\mu_f = \frac{\text{mass of fuel reacted}}{\text{mass of fuel input}} \quad (13)$$

This value, which can be estimated at 0.95, takes into account any fuel that is fed to the cell but cannot be used. This results in the following equation for efficiency (Larminie and Dicks, 2003):

$$\text{efficiency} = \mu_f \frac{V_c}{1.48} * 100\% \quad (14)$$

2.2.3 The Nernst Equation

It has already been said that the Gibbs free energy changes with temperature, but it also changes with the pressure and concentration of the reactants. In the overall reaction of the fuel cell,

$$H_2 + \frac{1}{2}O_2 \rightarrow H_2O \quad (15)$$

the Gibbs free energy will be affected by the activity of the water, hydrogen, and oxygen. Activity is designated by the symbol a. For ideal gases,

$$a = \frac{P}{P^0} \quad (16)$$

Where P^0 is standard pressure, 0.1 MPa, and P is the partial pressure of the gas. Accounting for changes in activity, for thermodynamic reasons, the equation for the Gibbs free energy change of this reaction becomes

$$\Delta\bar{g}_f = \Delta\bar{g}_f{}^0 - RT\ln\left(\frac{a_{H_2}\cdot a_{O_2}^{\frac{1}{2}}}{a_{H_2O}}\right) \quad (17)$$

It can be seen from this equation that if the activity of the reactants increases, more energy is released ($\Delta\bar{g}_f$becomes more negative), and if the activity of the product increases, less energy is released (Larminie and Dicks, 2003).

To relate this with voltage, it can be substituted into the equation for EMF

$$V = \frac{-\Delta\bar{g}_f}{2F} \quad (18)$$

to result in

$$V = V^0 + \frac{RT}{2F}\ln\left(\frac{a_{H_2}\cdot a_{O_2}^{\frac{1}{2}}}{a_{H_2O}}\right) \quad (19)$$

where V^0 is the EMF at standard pressure, found earlier.

2.2.4 The Effect of Gas Concentration on Efficiency

Assuming that the gases in the fuel cell are behaving ideally, the activities can be defined by

$$a_{\mathrm{H}_2} = \frac{P_{\mathrm{H}_2}}{P^0},\ a_{O_2} = \frac{P_{O_2}}{P^0},\ a_{H_2O} = \frac{P_{H_2O}}{P^0} \quad (20)$$

and if the pressures are given in bar, then $P^0 = 1$ and

$$V = V^0 + \frac{RT}{2F}\ln\left(\frac{P_{H_2}\cdot P_{O_2}^{\frac{1}{2}}}{P_{H_2O}}\right) \quad (21)$$

Isolating the hydrogen pressure term gives

$$V = V^0 + \frac{RT}{2F}\ln\left(\frac{P_{O_2}^{\frac{1}{2}}}{P_{H_2O}}\right) + \frac{RT}{2F}\ln(P_{H_2}) \quad (22)$$

If the hydrogen partial pressure changes from P_1 to P_2 bar, the expected voltage change can be calculated by the following equation

$$\Delta V = \frac{RT}{2F}\ln(P_2) - \frac{RT}{2F}\ln(P_1) = \frac{RT}{2F}\ln\left(\frac{P_2}{P_1}\right) \quad (23)$$

For example, changing from pure hydrogen to a 50% mixture of hydrogen and carbon dioxide at 200°C in a phosphoric acid fuel cell will reduce the voltage by about 0.015 V (Larminie and Dicks, 2003).

2.2.5 Stacks and the Bipolar Plate (Interconnect)

Because each individual fuel cell can only produce about 0.7 V at useful currents, oftentimes cells must be connected in order to produce a necessary voltage. While cells could be connected in series, this would mean that the electrons must flow across the face of an electrode, be collected at a point on the edge, and then move onto the next cell. To avoid the voltage drop associated with connecting fuel cells in series, a common method is to use a bipolar plate, which connects the entire surface of the cathode of a fuel cell to the anode surface of the next cell. The plates have grooves in them to deliver gas to the entire surface of the electrodes, while keeping the hydrogen and oxygen separated. Due to these channels, as can be seen in Figure 3 (Resin systems for advanced graphite composite fuel cell bipolar plates, 2010), the electric current can pass directly through the cells rather than over each electrode in succession (Larminie and Dicks, 2003).

Figure 3: Fuel Cell Bipolar Plate Channels

2.2.6 Causes of Voltage drop

As previously stated, a running fuel cell will not run at the theoretical OCV. The actual OCV will be less than calculated, and as the current density increases, the voltage will decrease. This is due to irreversibilities in the fuel cell, which are deviations from ideal operation Figure 4 shows the voltage for a typical PEM fuel cell (Matter, 2010).

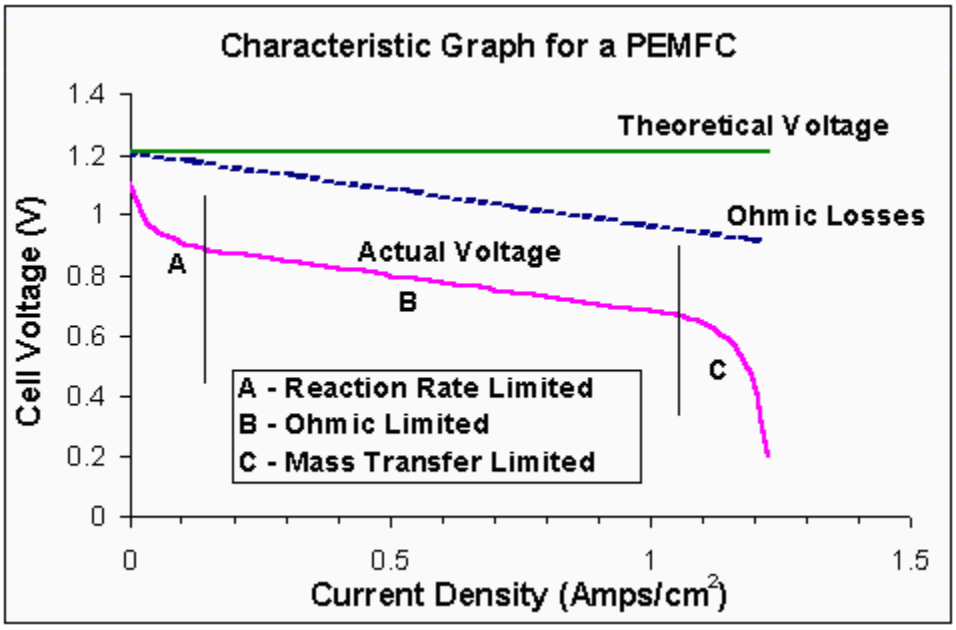

Figure 4: Characteristics Graph for a PEMFC

The first characteristic of a fuel cell that leads to voltage loss is activation energy. Some of the voltage created by the fuel cell is used to drive the chemical reactions at the electrodes. Ohmic losses are due to the electrical resistance of the electrodes and electrolyte, and a third type of losses, mass transport or concentration losses, take place when the fuel gases are consumed at the electrodes. For example, as oxygen is consumed at the cathode, the concentration of oxygen in the air will decrease. This decrease can be quite small, but it depends upon the current being taken from the fuel cell and how the air is able to circulate around the cathode. The same goes for hydrogen at the anode. These voltage losses are explored to a greater extent in section 3.2.4 Theoretical Cell Voltage.

2.2.7 Obstacles to Fuel Cell Development

The primary obstacle to any emerging technology is cost. PEMFC systems are priced at $73 per kilowatt while comparative gasoline powered vehicles are priced at $35 per kilowatt. The reason for this is that the PEM's catalysts (normally made of platinum) are extremely expensive. Research must be conducted in order to decrease the amount of catalyst needed or find a more economically priced alternative (Harper, 2008).

Degradation of the fuel cell due to frequent cycling on and off is another large obstacle in the development of fuel cells. PEMFC's must be developed which can operate at temperatures greater than 100°C and still function at freezing temperatures. Cyclical temperature fluctuations in conjunction with frequent startups and shut downs quickly degrade the fuel cells (Harper, 2008).

The hydration of the fuel cell is also an issue due to fluctuating temperatures. It is difficult to maintain a hydrated system in sub-zero temperatures and above 80°C (Harper, 2008).

2.3 Literature Review

This section will discuss how contaminants in the hydrogen stream entering a PEM fuel cell have been found to affect the fuel cell itself, and how the damage is examined through voltage monitoring and impedance spectroscopy.

2.3.1 The effect of carbon monoxide on PEM fuel cells

Traces of carbon monoxide are often found in hydrogen streams if they are produced by conventional steam reforming of hydrocarbons (Bonnet, Ronasi and Pereira, 2009), and they can permanently damage platinum anodes on PEM fuel cells. Platinum adsorbs carbon monoxide much more readily than hydrogen, and previous experiments have shown that with concentrations of 10 to 100 ppm of carbon monoxide, the catalyst surface becomes nearly completely covered with CO (Bonnet, Ronasi and Pereira, 2009). The scientists ran an experiment to determine whether or not this holds true for lower concentrations of 5 ppm or less of carbon monoxide in the hydrogen stream.

To begin the experiment, pure hydrogen was fed to the fuel cell for an hour while the cell voltage was recorded at a fixed current density. Next, hydrogen polluted with CO was fed to the anode, usually for several hours, until steady state was reached, and then pure hydrogen was fed once again, recording the cell voltage variation continuously. At the end of each of these periods, impedance spectra were obtained as well. The voltage variation and electrochemical impedance were both used to characterize the damage done to the fuel cell.

This experiment found that the effect of carbon monoxide pollution on the cell voltage corresponded directly with the concentration of the pollutant. With CO concentrations of 1 ppm, the voltage decrease was found to be 110 mV, while the drop increased to 260 mV when the concentration of CO was increased to 5 ppm. The speed of the decrease also depended on the concentration of the pollution. When the concentration of CO was low, the cell response wasn't

immediate and the voltage decreased over many hours. When the concentration was high, the cell responded faster and had a much sharper decrease in voltage. After repeated experiments using the CO contaminated streams, the voltage with pure hydrogen had decreased by 30 mV, so the damage caused by the CO was indeed found to be permanent (Bonnet, Ronasi and Pereira, 2009).

2.3.2 Investigation of the effect of CO on the hydrogen oxidation on the PEMFC anode surface

The investigation of PEM Fuel Cells operating with pure hydrogen feed for hydrogen oxidation and oxygen reduction is usually modeled as a two-fold process. The first part of the process is characterized by its fast kinetics and irreversibility is modeled by the Butler-Volmer equation. The second part is characterized by slow kinetics, as it is the almost irreversible process controlled by diffusion phenomena. However, the Butler-Volmer law greatly under predicts the resulting experimental values linking current density to overpotential. Hydrogen oxidation occurs on the smooth platinum surface of the catalyst plate. The mechanism for electrochemical hydrogen oxidation on a Platinum catalyst consists of two steps:

$$H_2 + 2M \Leftrightarrow 2MH \quad (24)$$

$$2MH \Leftrightarrow 2M + 2H^+ + 2e^- \quad (25)$$

The expression to calculate Ohmic resistance of charge transfer is typically (Lapicque, 2009):

$$r_{tc} = \frac{RT}{2Fi} * tanh * [(\frac{2F}{RT}) * \eta] \quad (26)$$

When this equation is used to model an experiment conducted with appreciable values of anode overpotential (ie: concentrations of CO greater than 2ppm) the r_{tc} equation would result in a resistance of charge of 0.03 Ωcm^{-2} which is nearly 25 times lower than the experimental value

of 0.8 Ωcm^{-2}. Research is currently underway to determine a more accurate method to predict the resistance of charge in a fuel cell supplied with an H_2 – CO mixture.

2.4 Background for Experimental Methodology

2.4.1 Galvano Electrochemical Impedance Spectroscopy (Frequency Response Analysis)

The impedance spectrum allows for the analysis of the fuel cell though the application of a small alternating current perturbation signal to the cell. The AC perturbation signal is applied with a constant voltage and current. The AC signal frequency is typically varied between 10 kHz and 100 mHz. The system response is measured as a function of the AC frequency variation, from which the impedance of the system can be determined (Dotelli, Omati and Gallo Stampino, 2009).

Impedance spectroscopy is run under varying current densities. At low current density the impedance spectrum exhibits a single arc as a result of the charge transfer. At medium current density a smaller, low-frequency arc due to the mass transfer resistance is notable along with the larger charge transfer arc. The intercept of the high frequency with the Z axis represents the resistance of both the charge transfer and mass transfer resistances (contact resistances) (Dotelli, Omati and Gallo Stampino, 2009).

Impedance spectroscopy is used to characterize multiple parameters of the electrical response of the system such as the electrolyte resistance, kinetic and mass transport resistance. Impedance spectroscopy in a fuel cell is focused on the dominant loss factors of the fuel cell and their relation to controlled variables such as the current density, voltage humidification and fuel composition (Choi, Howze and Enjeti, 2006). The system used for electrical analysis for this project was similar to the system diagram in Figure 5 (Choi, Howze and Enjeti, 2006).

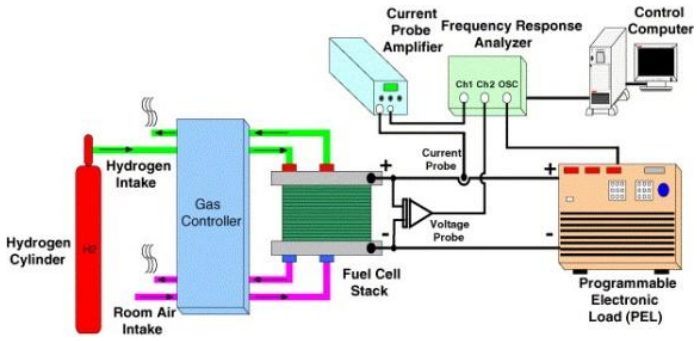

Figure 5: Experimental Impedance Spectroscopy Frequency Response Analyzer Setup

Impedance spectroscopy is a type of frequency response analysis. It is customary to model the fuel cell with an equivalent DC electric circuit such as shown in Figure 6.

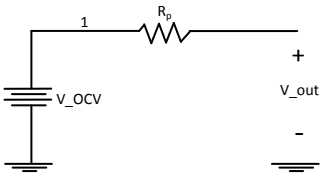

Figure 6: DC-Circuit

V_{OCV} stands for the potential of the open circuit fuel cell. In an open circuit no current requirement exists. R_p in this case stands for the overall cell resistance which is assumed to be constant with the current. Thus when the circuit is closed and a load is applied, current will begin to flow and a potential drop will exist across R_p. The resulting voltage can be calculated using Ohms law and will be dependent on the value of R_p and the current load.

$$V_{load} = V_{OCV} - i_{load} \cdot R_p \qquad (27)$$

Unfortunately, the potential losses within a fuel cell are not constant – charge transfer, kinetic and mass transport each affect the fuel cell resistance at different points in the cell at different frequencies. Four types of AC equivalent circuits allow for a more accurate, albeit increasingly complex representation of the fuel cell for impedance modeling:

1. RC-circuit
2. RLC-circuit

3. Nerst Impedance
4. Warburg Impedance

RC-Circuit

The RC-circuit is composed of a capacitor and resistor connected in parallel to represent the capacitance of the double layer electrode and the ohmic resistance of the fuel cell, respectively, as shown in Figure 7.

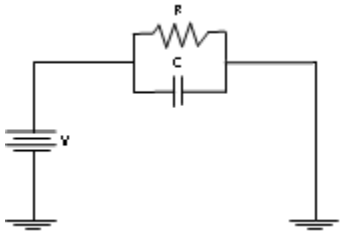

Figure 7: RC-circuit

Impedance in an RC-circuit is defined as:

$$Z_{RC}(j \cdot \omega) = \frac{R}{1+j \cdot \omega \cdot R \cdot C} \qquad (28)$$

The RC-circuit describes fuel cell impedance graphed in a Nyquist plot as a semi-circle called a capacitive loop as shown in Figure 8 (Danzer and Eberhard, 2009).

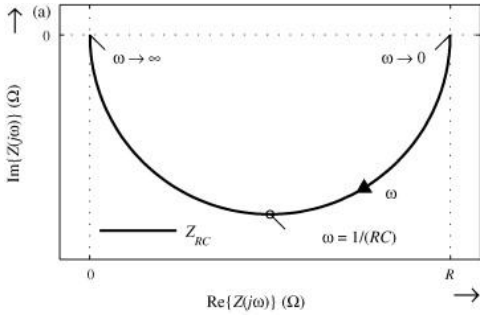

Figure 8: Impedance of RC-circuit

Figure 8 demonstrates that as the frequency ω approaches zero the impedance of the RC-circuit approaches the axis where Z_{RC} is equal to the resistance R.

$$Z_{RC}\left(j\cdot\left[\omega=\frac{1}{R\cdot C}\right]\right)=\frac{R}{1+j\cdot\omega\cdot R\cdot C}=R \quad (29)$$

As the frequency moves to infinity the magnitude of the impedance approaches zero (Danzer and Eberhard, 2009).

$$Z_{RC}(j\cdot[\omega=\infty])=\frac{R}{1+j\cdot\omega\cdot R\cdot C}=0 \quad (30)$$

RLC-Circuit

The RLC-circuit includes an inductor and resistor connected in series in addition to the parallel resistor and capacitor found in the RC-circuit. The equivalent circuit diagram is displayed below in Figure 9, where *L* stands for the inductance the fuel cell experiences at high frequencies, while R_b and R_a represent the activation resistance and electrolyte resistance respectively. *C* represents the capacity of the electrical double layer.

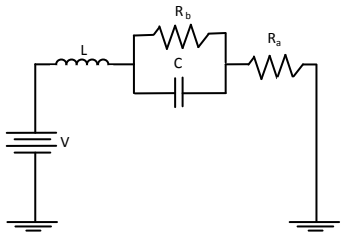

Figure 9: Equivalent RLC-Circuit

Impedance in an RLC-circuit is more complicated than that of the RC-circuit. RLC-circuit impedance is defined as:

$$Z_{RLC}(j\cdot\omega)=\frac{R_a\cdot R_b+j\cdot\omega\cdot R_a\cdot L}{R_a+R_b+j\cdot\omega\cdot R_a\cdot R_b\cdot L+(j\cdot\omega)^2\cdot R_a\cdot L} \quad (31)$$

Z_{RLC} exhibits a second order response in relation to $j\omega$ which results in an inductive loop which is added to the capacitive lop of the RC circuit. The inductive loop occurs at low frequencies in a fuel cell and indicates a sinusoidal change in membrane resistance resulting

from a cyclical hydration and dehydration of the polymer electrolyte. This effect is shown below in Figure 10 (Danzer and Eberhard, 2009).

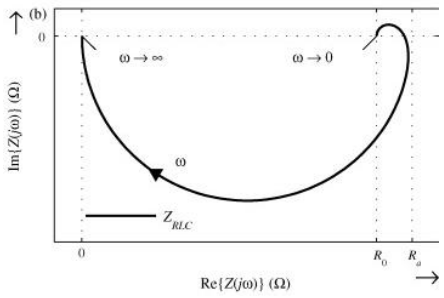

Figure 10: Impedance of RCL-circuit

Nernst Impedance

The Nernst impedance model is used to describe the diffusion process. It is modeled by the Warburg impedance model is used in addition to the Nernst model in order to describe the diffusion process. The Warburg impedance is modeled by the equation:

$$Z_W(j \cdot \omega) = R_{diff} \frac{tanh(\sqrt{\tau_d \cdot j \cdot \omega})}{\sqrt{\tau_d \cdot j \cdot \omega}} \quad (32)$$

where R_{diff} is the diffusion resistance and τ_d is the diffusion time constant in seconds. As the frequency decreases to zero the Nernst resistance equals the diffusion resistance and the slope of the line moves towards π/4 radians.

$$R_{diff} = Z_N(j \cdot \omega = 0) \quad (33)$$

An example of the Warburg impedance spectrum can be seen in Figure 11.

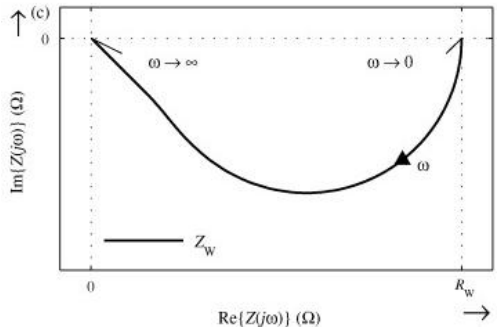

Figure 11: Warburg Impedance Spectrum

Overall Impedance

The overall impedance of a fuel cell is determined by the summation of the Ohmic resistance *R*, the two impedances for the two arcs of the Nyquist plot and the inductor *L* as shown below:

$$Z_{FC}(j \cdot \omega) = R + Z_1(j \cdot \omega) + Z_2(j \cdot \omega) + Z_L(j \cdot \omega) \quad (34)$$

When the frequency approaches zero the spectrum intercepts the real axis and is equal to the static resistance of the cell.

$$R = Z_{FC}(j \cdot \omega = 0) = R + Z_1(0) + Z_2(0) + Z_L(0) \quad (35)$$

The RC-circuit, RLC-circuit, Nernst impedance and Warburg impedance models agree in their description of the Ohmic resistance and cable inductance. However, they differ in their description of the behavior of the two Nyquist plot arcs and the analogous dominant impedance within the fuel cell. The most common practice in identifying the dominant impedance within a fuel cell is to fit the Impedance Spectroscopy data to an existing model and minimize the errors between the experimental data and the model. It is possible to design a model for a specific fuel cell, but it is more common to use an existing model.

Concerning this project, the experimental data was collected using a frequency response analyzer over a frequency range of 10 kHz to 100 mHz. Fifty data points were collected during each impedance spectroscopy. This data was input into a Microsoft Excel spreadsheet which allowed the data to be modeled based upon twelve parameters. The Excel model consisted of a Bode plot, a Nyquist plot and an enlarged Nyquist plot. An example Nyquist plot can be seen in Figure 12.

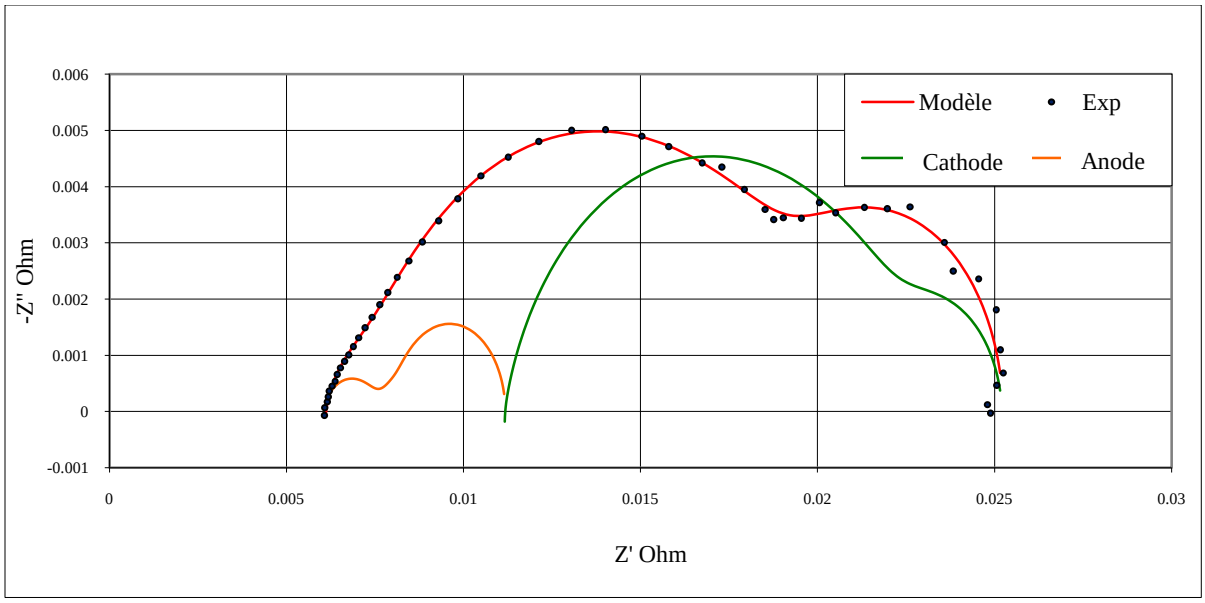

Figure 12: Example Nyquist Plot

The degree of accuracy in the fitting process was determined by the minimization of the differences between the experimental data and the model. The twelve parameters were then ready for comparative analysis to other experimental runs.

2.4.2 Water Balance

To analyze the flow of water in the cell, one of the parameters we looked at was the water transport coefficient, which is:

$$\alpha = \frac{F^A_{H_2O,out} - F^A_{H_2O,in}}{\left(F^A_{H_2O,out} - F^A_{H_2O,in}\right) - \left(F^C_{H_2O,out} - F^C_{H_2O,in}\right)} \quad (36)$$

In the experiments described in this paper, there is no water introduced in the anode, so $F^A_{H_2O,in} = 0$ and the equation can be simplified to

$$\alpha = \frac{F^A_{H_2O,out}}{F_{H_2O,prod}} \quad (37)$$

When the coefficient is less than zero, which will only happen when there is water introduced in the anode feed, the net flow of water is going from the anode to the cathode. In other words, the diffusion flux is in the same direction as that of electro-osmosis (anode to

cathode) or, it might be the opposite but it is less than the absolute value of the flow of electro-osmosis.

If the water transport coefficient is equal to zero, the flow of electro-osmosis and diffusion are equal and opposite. There is no net flow, and it is as if the membrane is impermeable to water.

Lastly, if it is greater than zero, the net flow of water goes from the cathode to the anode. The diffusion flux is negative and greater than the electro-osmosis flow. These characteristics are visually described in Figure 13.

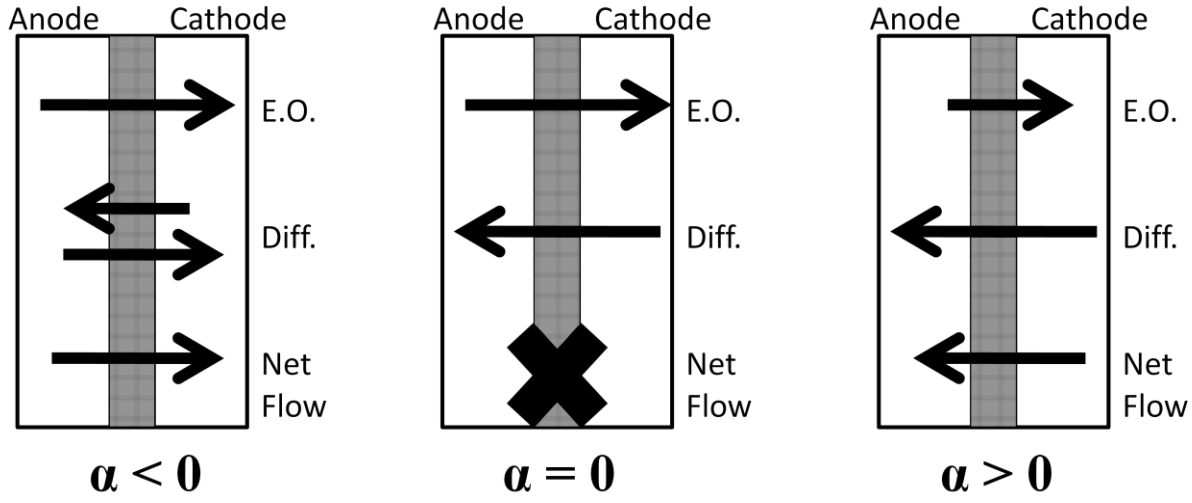

Figure 13: Water Transport Coefficient Diagram

The other parameter we analyzed was the water ratio at the electrodes. This is the ratio between the water fraction and the saturated water fraction. When below 1, this value signifies that there is only water vapor present, and it can also be referred to as the relative humidity. When the water ratio is above 1, that means that there is liquid water present at the electrode, which signifies flooding in the fuel cell.

3.0 Methodology

The experimental procedure for this project was controlled by the computer program EC-Lab Express V5.20 Beta. This program allowed us to vary our test parameters and then monitored the resulting polarization curve or Impedance Spectroscopy Curve. The current density was set at 0.12 A/cm^2,± 0.24 A/cm^2 and 0.36 A/cm^2 respectively.

3.1 Equipment

In this section the usage of the fuel cell bench hardware and accompanying software are discussed. The fuel cell assembly used in our project in LSGC, ENSIC, Nancy, France consisted of a fuel cell bench with the following hardware listed in

Figure 14 and described in the following sections.

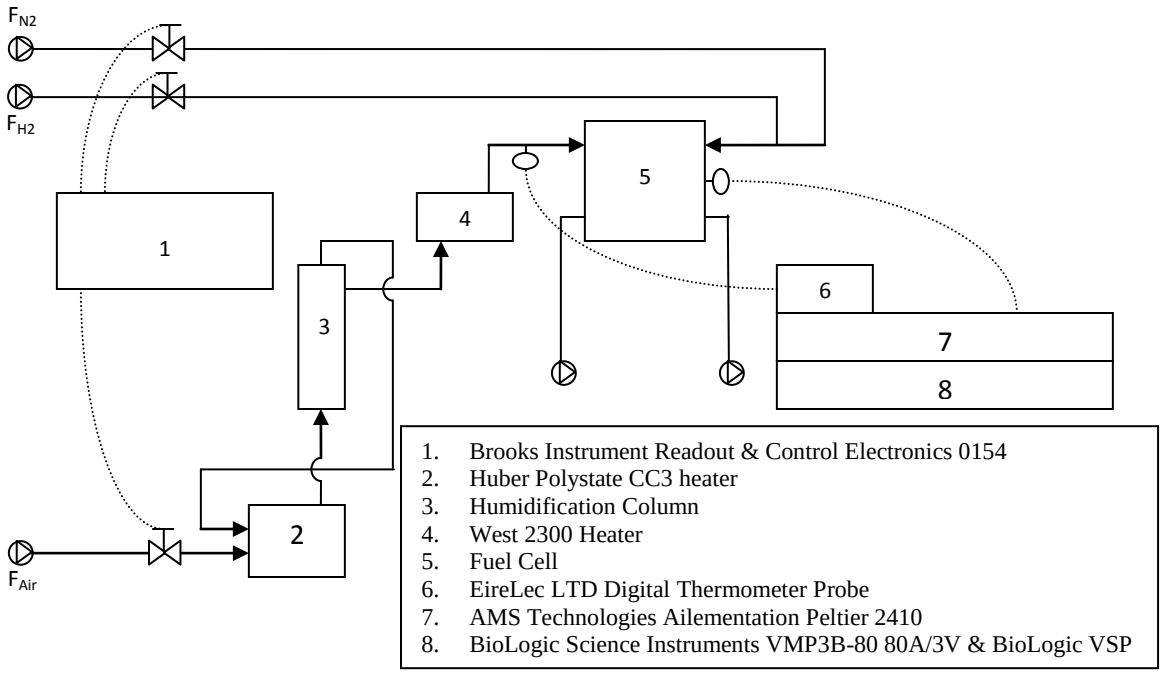

Figure 14: Fuel Cell System Schematic

Figure 15 provides a photograph of the fuel cell bench and associated hardware. The gas flow rate controller is at the upper left, the temperature readouts are at the upper right, the fuel

cell is just above center, the water collection bottles are at the bottom center, and the electrical analysis equipment is on the bottom right.

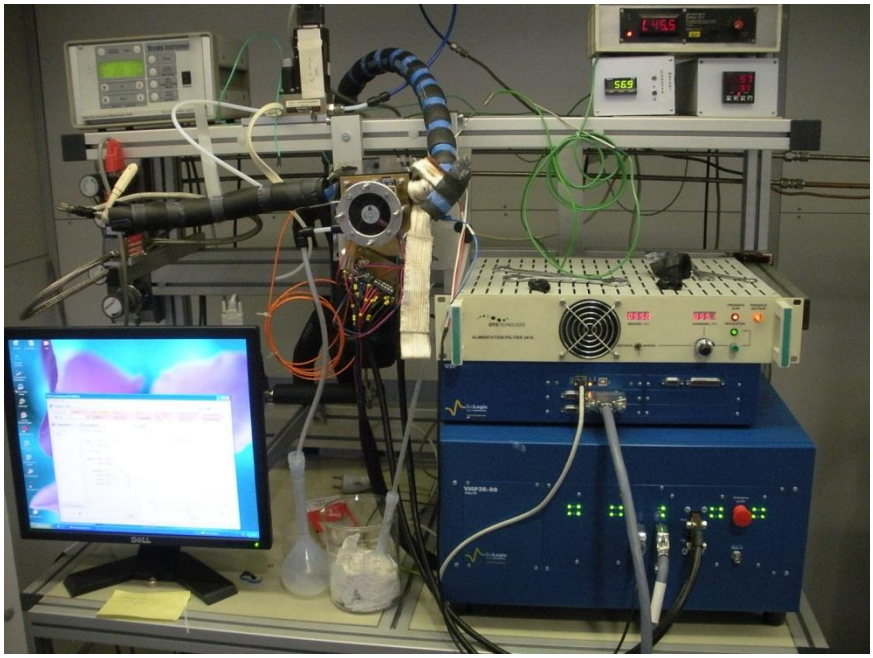

Figure 15: Fuel Cell Assembly and Associated Hardware

The software programs used were EC-Lab V9.94, EC-Lab Express V5.20 Beta and Microsoft Excel 2007.

3.1.1 Gas Supply and Manipulation

The fuel cell gas supply was controlled with the Brooks Instrument Readout & Control Electronics 0154 as shown in Figure 16 below.

Figure 16: Gas Flow Rate Controller

Air, hydrogen and nitrogen were introduced to the fuel cell at calculated flow rates calculated using Faraday's law and the reaction stoichiometry based upon the desired conditions. The air was comprised of 21% oxygen and 79% Nitrogen. Table 1 shows the required flow rates at STP for the desired condition of the fuel cell.

H2	Flow Rate	3A	6A	9A
100% λ=1.5	$F_{H2}\ (^{mL}/_{min})$	27.5	55	82
	$F_{air}\ (^{mL}/_{min})$	160	300	435
50%	$F_{N2}\ (^{g}/_{h})$	1.25	2.8	4.35
20%	$F_{N2}\ (^{g}/_{h})$	5.9	12.1	18.15
10%	$F_{N2}\ (^{g}/_{h})$	13.65	27.05	39.57
100% λ=3	$F_{H2}\ (^{mL}/_{min})$	55	110	164
	$F_{air}\ (^{mL}/_{min})$	160	300	435
100% λ=7.5	$F_{H2}\ (^{mL}/_{min})$	137.5	275	410
	$F_{air}\ (^{mL}/_{min})$	160	300	435

Table 1: Test Conditions

The flow required to provide the exact amount of gas to provide the target current density is at a stoichiometric coefficient of one. Thus a stoichiometric coefficient of 3 would be a flow rate three times higher than that required to produce the desired current density. In order to avoid providing less fuel than required for the desired current density, the basic stoichiometric coefficient or lambda used was 1.5. From Table 1 it can be observed that dilution cases were

only performed with the stoichiometric coefficient of 1.5. Stoichiometric coefficients 3 and 7.5 were also tested. The air flow passed through the provided humidification column heated by the West 2300 Heater in order to attain the desired relative humidity. The humidification column can be seen in Figure 17.

Figure 17: Humidification Column

It is known that flooding occurs when the relative humidity rises close to or above 70% in the fuel cell and depends on the stoichiometric factor and the water produced by the fuel cell. For nominal fuel cell conditions the relative humidity at the cathode was 62% and at the anode was 0% at a temperature of 55˚C.

3.1.2 Electrical Control System

The electrical control system software consisted of EC-Lab© V9.94 and EC-Lab© Express V5.20 Beta. The Express program was used for the majority of the experiments as its user interface is easy to use. The software was used to control the current load on the fuel cell and perform impedance spectroscopy. The detailed description of the use of these programs will be discussed in the impedance spectroscopy section of the Methodology.

3.1.3 The Membrane Electrode Assembly (MEA)

The fuel cell used for these experiments was a 25 cm^2 cell. The cell's normal operating conditions were at 55˚C, a relative humidity of 62% in the cathode and 0% in the anode, and a pressure of one atmosphere. The fuel cell catalyst is a Platinum/Ruthenium 0.45 mg/cm^2 at the anode, and Platinum 0.4 mg/cm^2 at the cathode supported on carbon particles. The ruthenium resists carbon monoxide poisoning of the platinum catalyst. The membrane is a polymer polytetrafluoroethylene with a thickness of 18 micrometers. The cathode and anode internal manifolds were arranged as in Figure 18 with the channels in dark grey and plate backing in light grey.

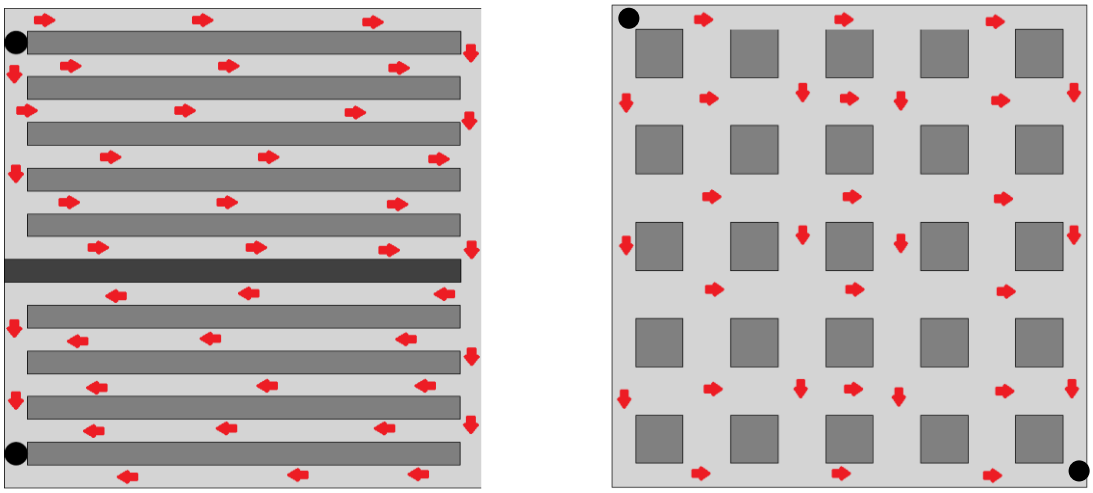

Figure 18: Anode & Cathode Respective Bipolar Plate Configuration

3.2 Experimental

3.2.1 Hydrogen Oxidation

To study the voltage and resistance of the fuel cell, tests were run using various parameters. First, using pure hydrogen fuel at the anode and air at the cathode, chronopotentiometry (CP) was used to obtain a voltage graph. The determined current was applied, and then when the voltage had reached steady state after about 15 minutes, water collection bottles were placed under the anode and cathode exit tubes. After an hour of water

collection, the CP was stopped and the bottles were removed. Using Galvano Electrochemical Impedance Spectroscopy (GEIS), two impedance spectra were then obtained. Meanwhile, the mass of the water collected at each electrode was recorded and the bottles were dried to prepare for the next experiment. After the GEIS was complete, the fuel gas flow rates were changed and a new CP was started.

This procedure was repeated about four or five times a day, applying a different current to the fuel cell each time. The currents tested were 3, 6, and 9 A, which on a 25 cm^2 fuel cell convert to current density values of 0.12, 0.24 and 0.36 A/cm^2. Overnight, the fuel cell was usually left running at 6 A.

Once these tests were completed using pure hydrogen as the fuel gas, some experiments were performed using hydrogen diluted with nitrogen. The dilution cases were 50%, 20%, and 10% hydrogen, and were carried out at the same current density values as the pure hydrogen case.

Lastly, the experiments were also performed using a range of stoichiometric coefficients (λ). For example, if hydrogen is being consumed by the fuel cell at a rate of 3×10^{-5}mol/s, a stoichiometric coefficient of 1.5 would mean that hydrogen is being fed to the fuel cell at a rate of 4.5×10^{-5}mol/s. This allows for an excess of hydrogen to be present at the electrode, which may prevent flooding. The stoichiometric coefficients tested were 1.5, 3, and 7.5 for hydrogen, while keeping the air stoichiometry constant at 3.

3.2.2 Galvano Electrochemical Impedance Spectroscopy: Nyquist Curve Modeling

The EC-Lab© programs were used to run Galvano Electrochemical Impedance Spectroscopy tests on the fuel cell. The experiments were conducted over a frequency range from 10 kHz to 100 mHz. The data was then imported into a Microsoft Excel spreadsheet where

it was fitted against a Bode plot and Nyquist plot with 12 parameters. The first step to find the best fit of the model to the theoretical data was to adjust manually the following values:

- R_{ohm}: Ohmic Resistance
- R_{ct}: charge transfer resistance for cathode
- Q_c: pseudo capacity for cathode
- n_c: cathode constant
- R_{dc}: $R_{diff,C}$: diffusion resistance cathode
- τ_{dc}: time constant in seconds for cathode
- $R_{ct,a}$: charge transfer resistance for cathode
- Q_a: pseudo capacity for anode
- n_a: anode constant
- R_{da}: $R_{diff,A}$: diffusion resistance anode
- τ_{da}: time constant anode
- L: inductance (only at high frequency)

The data was fitted against the theoretical model using a Microsoft Excel program. In order to ensure an accurate fit the square of the differences between the theoretical model and the experimental data was minimized.

$$\text{Best Fit} = \min \sum_{\omega=10\text{ kHz}}^{\omega=100\text{mHz}} \sqrt{\left(Z_{FC_{exp}} - Z_{FC_{theory}}\right)^2} \quad (38)$$

The Nyquist diagram was created by plotting the imaginary impedance *-Z"/ohm* as a function of the real *Z'/ohm*. Figure 19 is a Nyquist diagram in the process of being fitted to the model. Above the diagram is an equivalent circuit showing what parts of the Nyquist diagram each parameter affects. The anode and cathode capacitors represent the double layer of the two electrodes. R_{ohm} stands for the electrolyte membrane of a finite conductivity.

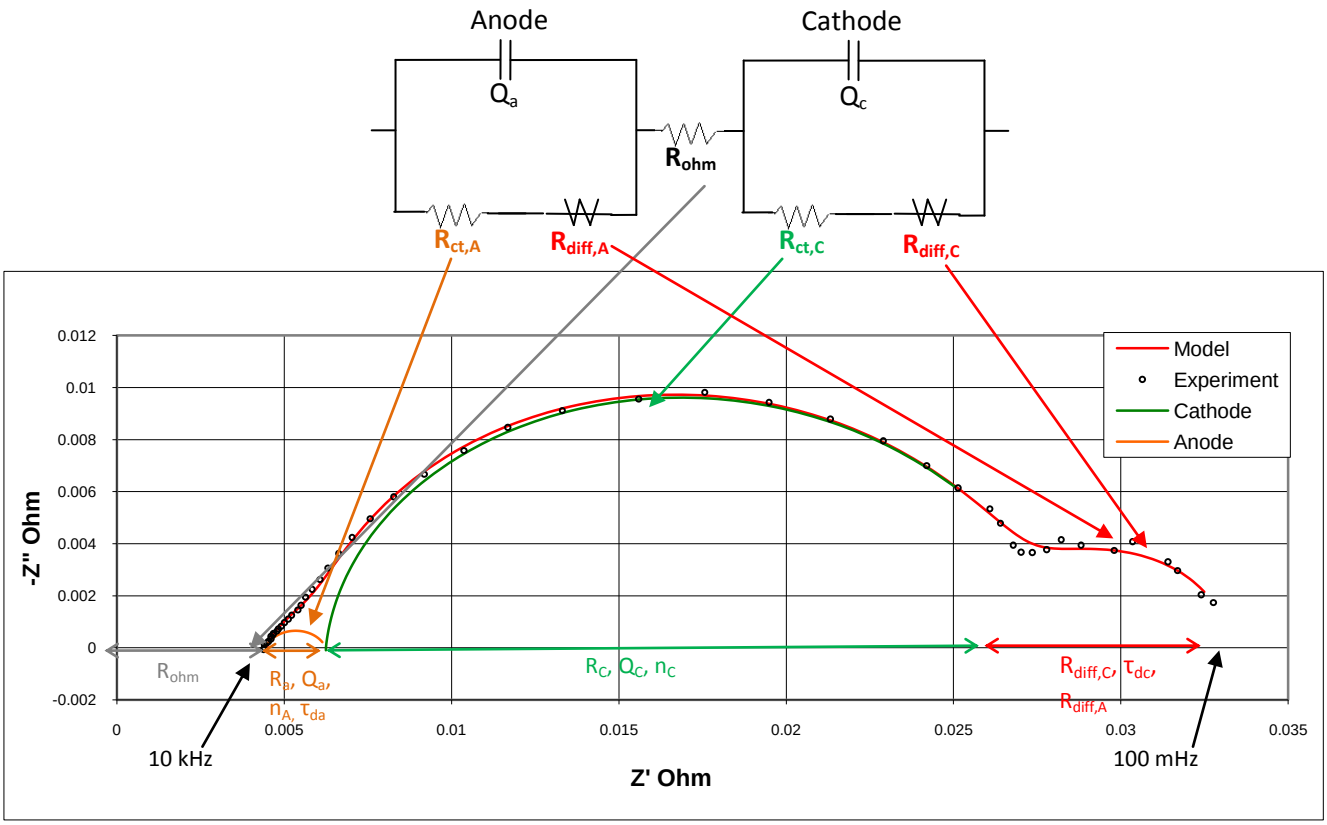

Figure 19: Example of Nyquist Diagram with Equivalent Circuit of the Fuel Cell

The experimental graph was first hand fit with the model before using the data solver function in Excel in order to correctly describe the experiment. The high frequency region is characterized by the manipulation of R_{ohm}, R_a, Q_a, and n_a. The ohmic resistance was adjusted to align the point where the experimental graph in the Nyquist model intersected the x axis. A lower R_{ohm} value shifted the graph to the left while a larger value shifted it to the right. The charge transfer resistance for the cathode affected the diameter of the first loop of the Nyquist plot. A larger value would yield a larger arc, while a smaller value would cause a tighter curve. The cathodic capacitance and cathode constant were then adjusted to modify the height of the curve. These values were fitted together as very small changes in either parameter result in large changes in the ability of the other parameter to impact the curve. The middle frequency region is fitted by the manipulation of the variables R_c, Q_c and n_c. Finally the low frequency region is

controlled by the manipulation *of* $R_{diff,C}$, τ_{dc}, $R_{diff,A}$, and τ_{da}. The value of diffusion resistance in the cathode $R_{diff,C}$ affected the height and breadth of the second curve. The cathode time is an expression of δ/D which is the length of diffusion divided by the diffusion coefficient. This was manipulated to better fit the data.

The constant L is used to compensate for the inductance experienced by the fuel cell due to the large amount of metal and wires which surround the unit.

$$\text{Inductance} = 2 \cdot \pi \cdot \omega \cdot j \cdot L \qquad (39)$$

The value of n_a was fixed to 0.8 as it is very difficult to fit twelve parameters with accuracy. By fixing n_a it was possible to accurately model the other eleven parameters. Also, the larger arc of the Nyquist plot overshadows the smaller arc and inhibits the model's ability to determine the value for n_a. It was also known that values for n_a for the platinum-Ru catalyst being used for this experiment vary between 0.8 and 0.9. It was thus decided that n_a should be fixed at 0.8 for the entirety of the project so as to ensure consistency within the fitting.

The solver in Microsoft Excel was used to fit the middle, upper, and lower parameters of the graph in groups before the eleven parameters (excluding L) were fitted simultaneously to achieve the best accuracy.

The fitting process was repeated as many times as desired to acquire an acceptable level of similarity between the experimental data and the model. The data was then ready for analysis.

3.2.3 Exchange Current Density

Exchange current density, or i_0, is a value used to describe the rate of electron transfer between an analyte and an electrode at equilibrium potential. The exchange current density depends on the roughness of the electrode surface, its catalytic properties, presence of oxides, water, the concentration of the reactive species, the composition of the electrode and electrolyte and the temperature. The exchange current density for the anode was found by fitting $R_{ct,a}$ to the

model value found in the Nyquist curve modeling. The exchange current density value was solved for by minimizing the differences between the calculated $R_{ct,a}$ and the modeled $R_{ct,a}$ at various water densities.

$$R_{ct,a} = \frac{1}{ib_a}\tanh\left[\operatorname{arcsinh}\left(\frac{\mathrm{i}}{2\mathrm{i}_{0,a}}\right)\right] \quad (40)$$

$$i = \text{current density } {}^{A}/_{cm^2} \quad (41)$$

$$b_a = \text{Tafel Slope} = \frac{2F}{RT} = 70.73\ V^{-1} \quad (42)$$

$$i_{0,a} = \text{Exchange Current Density } {}^{A}/_{cm^2} \quad (43)$$

The Tafel slope is a temperature dependent constant also using the Faraday's number. The anode exchange current density ($I_{o,a}$) will be calculated and the relation of lambda and percent hydrogen flows will be compared for 100, 50, 20 and 10% hydrogen verses lambdas 1.5, 3 and 7.5. The exchange current density value for 100% hydrogen will also be used to calculate the theoretical cell voltage at various imposed currents and compare that value to the actual cell voltage.

3.2.4 Theoretical Cell Voltage

The theoretical cell voltage is useful in analyzing the performance of the fuel cell. Two different equations were used to calculate the theoretical cell voltage of the fuel cell. The first set of equations was taken from Class Notes (Datta, 2010).

$$V_{theoretical} = V_0 - \eta_a + \eta_c - \eta_{EL} - R_{ohm}i \quad (44)$$

$$V_0 = 1.22 - 0.00085(T - 298.15) + \frac{RT}{2F}ln\left(\frac{P_{H_2}P_{O_2}^{1/2}}{P_{H_2O}}\right) \quad (45)$$

$$\eta_a = \left(\frac{RT}{\alpha_a^* v_{Ae}^* - F}\right)\sinh^{-1}\left[\frac{1}{2}\left(\frac{{}^{i_A}/_{i_{A,o}}}{1-{}^{i_A}/_{i_{A,L}}}\right)\right] \quad (46)$$

$$\eta_c = \left(\frac{RT}{\alpha_C^* v_{Ce}^* - F}\right) \sinh^{-1}\left[\frac{1}{2}\left(\frac{{}^{(i_C + i_{C,x})}/_{i_{C,o}}}{1 - {}^{(i_C + i_{C,x})}/_{i_{A,L}}}\right)\right] \quad (47)$$

$$\eta_{EL} = i_{EL}\left(\frac{L_{EL}}{\sigma_{EL}}\right) \quad (48)$$

The combined equations once V_o has been calculated result in the following equation:

$$V_{theoretical} = V_0 - \left(\frac{RT}{\alpha_a^* \alpha_{Ae}^* - F}\right) \sinh^{-1}\left[\frac{1}{2}\left(\frac{{}^{i_A}/_{i_{A,o}}}{1 - {}^{i_A}/_{i_{A,L}}}\right)\right] + \left(\frac{RT}{\alpha_C^* \alpha_{Ce}^* - F}\right) \sinh^{-1}\left[\frac{1}{2}\left(\frac{{}^{(i_C + i_{C,x})}/_{i_{C,o}}}{1 - {}^{(i_C + i_{C,x})}/_{i_{A,L}}}\right)\right] - i_{EL}\left(\frac{L_{EL}}{\sigma_{EL}}\right) - R_{ohm} i \quad (49)$$

The following values for parameters were fitted to allow for accurate description of the data by the theoretical equation.

Component	Parameter	Value	Units
Open Cell Voltage :	V_0	1.1925	V
Anode :	α_a^*	0.75	
	v_{Ae^-}	3.2	
	F	96485	
	$i_{A,0}$	0.142	A/cm^2 PT
	$i_{A,L}$	6	A/cm^2 MEA
Cathode :	α_c^*	0.5	
	v_{ce^-}	-1.1	
	$i_{c,0}$	0.0000089	A/cm^2 PT
	$i_{C,L}$	0.95	A/cm^2 MEA
	$i_{C,x}$	0	A/cm^2
Electrolyte :	L_{EL}	18	μm
	σ_{EL}	0	S/cm
Resistance :	R_{OHM}	0.00474	Ohm

Table 2: Parameters for Theoretical Voltage Calculation

The second theoretical voltage equations which were attained in Nancy France from the general practices of the ENSIC fuel cell laboratory were calculated with the following equation.

$$V_{theoretical} = V_0 - \eta_a - |\eta_c| - R_{ohm} i \quad (50)$$

The symbol η represents the cell overvoltage or electrode potential. Once the values for exchange current density for the anode and cathode and the Tafel slope for the anode have been calculated, the limiting current density for the cathode must be calculated. This can be done by setting a value for the limiting current density and resulting theoretical voltage against the

experimental cell voltage and minimizing the sum of the differences. The following equations illustrate how the theoretical voltage is calculated.

$$V_0 = 1.22 - 0.00085(T - 298.15) + \frac{RT}{2F} ln\left(\frac{P_{H_2} P_{O_2}^{1/2}}{P_{H_2O}}\right) \quad (51)$$

$$\eta_c = \sum \eta_{ct,c} + \eta_{diff,c} \quad (52)$$

$$\eta_a = \sum \eta_{ct,a} + \eta_{diff,a} \quad (53)$$

$$\eta_{ct,c} = \frac{1}{b_c} ln\left(\frac{i}{i_{0,c} - \frac{i}{i_{L,c}}}\right) \quad (54)$$

$$\eta_{ct,a} = \frac{1}{b_a} arcsinh\left(\frac{i}{2i_{0,a}}\right) \quad (55)$$

In the case of pure hydrogen, the value of $\eta_{diff,a}$ is neglected as it represents the overvoltage due to the diffusion resistance in the anode which is negligible.

$$\eta_{diff,c} = \frac{RT}{4F} ln\left(1 - \frac{i}{i_{L,c}}\right) \quad (56)$$

Thus the theoretical voltage is equal to the following equation and was calculated for a current density from 0.12 to 0.64 A/cm^2.

$$V_{theoretical} = V_o - \frac{1}{b_a} arcsinh\left(\frac{i}{2i_{0,a}}\right) - \left|\frac{1}{b_c} ln\left(\frac{i}{i_{0,c} - \frac{i}{i_{L,c}}}\right) + \frac{RT}{4F} ln\left(1 - \frac{i}{i_{L,c}}\right)\right| - R_{ohm} i \quad (57)$$

This value was then graphed against the experimentally found cell voltage and the fitting can yield an estimate for $i_{0,c}$.

3.2.5 Theoretical Charge Transfer Resistance

The theoretical anode and cathode resistance equations were taken from Class Notes (Datta, 2010). The parameter values are the same as those used in the theoretical voltage section above.

$$R_A = \frac{RT}{\left(2F\alpha_a^* v_{Ae-}^* i_{A,o}\right)\left(1-\frac{i}{i_{A,L}}\right)^2\sqrt{1+\frac{1}{4}\left(\frac{i/i_{A,o}}{1-i/i_{A,L}}\right)^2}} \quad \Omega cm^2 \qquad (58)$$

$$R_C = \frac{RT}{\left(2F\alpha_C^* v_{Ce-}^* i_{C,o}\right)\left(1-\frac{i}{i_{C,L}}\right)^2\sqrt{1+\frac{1}{4}\left(\frac{i/i_{C,o}}{1-i/i_{C,L}}\right)^2}} \quad \Omega cm^2 \qquad (59)$$

The theoretical resistances calculated with these equations will be compared to those found through the impedance spectroscopy fitting of data.

3.2.6 Open Cell Voltage

Using Equation 10 presented in the background section of this report, the theoretical OCV can be determined and compared to the actual OCV of the fuel cell. $\Delta\bar{g}_f$ varies with the operating temperature of the fuel cell, and Table 3 shows values that were obtained from Fuel Cell Systems Explained (Larminie and Dicks, 2003).

Form of water product	Temperature (°C)	$\Delta\bar{g}_f$ (kJ mol^{-1})
Liquid	25	-237.2
Liquid	80	-228.2
Gas	80	-226.1

Table 3: $\Delta\bar{g}_f$ values

Since the fuel cell was operating at a temperature of 45.4°C, these values were interpolated to obtain a value of -233.9 kJ mol^{-1}, which could then be used in Equation 10 to find the theoretical OCV.

3.2.7 Mass Balance Calculations

To monitor the water production of the fuel cell and ensure that the mass balance of the reactions occurring in the fuel cell area accurate, calculations were performed to compare the theoretical water produced to the water collected in the bottles. Because the reaction taking place at the anode is:

$$H_2 \rightarrow 2H^+ + 2e^- \qquad (60)$$

the flow rate of hydrogen consumed can be calculated by the following equation:

$$F_{H_2,cons} = \frac{I}{2F} \quad (61)$$

where F is Faraday's constant, 96485 Coulombs/mol, and I is the current being produced in the fuel cell. From here, the flow rate of hydrogen supplied to the fuel cell can be calculated using the stoichiometric coefficient, λ_A.

$$F_{H_2,in} = F_{H_2,cons} \cdot \lambda_A \quad (62)$$

In the cases where the hydrogen gas is diluted by nitrogen, the flow rate of nitrogen can be found using the mole fraction of hydrogen, y_{H_2}.

$$F_{N_2,in} = F_{H_2,in} \cdot \frac{1-y_{H_2}}{y_{H_2}} \quad (63)$$

It is known that none of the nitrogen reacts in the fuel cell, so the flow rate of nitrogen in will equal the flow rate of nitrogen exiting. The hydrogen fed to the fuel cell and the hydrogen consumed have already been calculated, so the exiting flow rate is the difference between these two numbers. Calculating the water exiting the anode is slightly more involved. The partial pressure of water in the anode exit can be calculated using Antoine's equation with T in degrees Celsius:

$$P_{H_2O}(atm) = \exp\left(11.6703 - \frac{3816.44}{273.15+T-46.13}\right) \quad (64)$$

By dividing the partial pressure by the total pressure, 1 atm, the fraction of water vapor in the water, hydrogen, and nitrogen exiting the anode (y_{H_2O}) is calculated, and from there the flow rate of water vapor can be found.

$$F_{H_2O\ vapor,out} = \frac{y_{H_2O} \cdot (F_{H_2,out} - F_{N_2,out})}{1-y_{H_2O}} \quad (65)$$

The flow rate of liquid water is calculated from the mass of water collected in the collection bottles divided by the time over which it was collected. Adding the liquid water and water vapor flow rates together gives the total amount of water exiting the anode.

Calculations on the cathode side of the fuel cell are similar. The reaction taking place is:

$$O_2 + 4e^- + 4H^+ \rightarrow 2H_2O \quad (66)$$

so the flow rates of oxygen being consumed by the fuel cell and supplied are:

$$F_{O_2,cons} = \frac{I}{4F} \quad (67)$$

$$F_{O_2,in} = F_{O_2,cons} \cdot \lambda_C \quad (68)$$

Since the fuel gas is air, 21% oxygen and 79% nitrogen, the flow rates of air and nitrogen entering the fuel cell are:

$$F_{air,in} = \frac{F_{O_2,in}}{0.21} \quad (69)$$

$$F_{N_2,in} = 0.79 \cdot F_{air,in} \quad (70)$$

The other component entering the fuel cell is water vapor. As previously mentioned, the air entering the fuel cell is humidified to prevent the fuel cell from drying out. The temperature of the humidifier affects the humidity of the air.

$$Relative\ Humidity = \frac{P^{sat}_{H_2O}(T_{humidifier})}{P^{sat}_{H_2O}(T_{cell})} \quad (71)$$

In the above equation, the relative humidity is fixed (at 0.62 except for the low/high humidity experiments), and the temperature of the cell is fixed at 55°C. The saturated pressure values can be calculated from Antoine's equation, and then the equation can be solved for the temperature of the humidifier.

Once this temperature is found, the partial pressure of water in the entrance air stream can be found using Antoine's equation, and divided by the total pressure of 1atm to find the fraction of water in the air fuel stream.

$$P^{sat}_{H_2O}(atm) = \exp\left(11.6703 - \frac{3816.44}{273.15+T-46.13}\right) \quad (72)$$

$$y_{H_2O,in} = \frac{P_{H_2O}^{sat}}{P_{total}} \quad (73)$$

The water entering the fuel cell at the cathode can then be calculated.

$$F_{H_2O\ vapor,in} = \frac{y_{H_2O} \cdot F_{air,in}}{1 - y_{H_2O}} \quad (74)$$

The next step was to find the flow rates of the materials exiting the cathode. Oxygen enters the fuel cell and is consumed in the reaction, so the exiting flow rate is simply the difference between the entering and consummation values. Nitrogen enters the fuel cell in the air and does not react, so the exiting value is equal to the entering value. The exiting flow rate of water is found in the same way as it was above for the anode.

To check the water balance around the fuel cell, the flow of water exiting the fuel cell can be compared to the total water entering and being produced in the fuel cell. The water entering the fuel cell has already been calculated, and the water produced in the fuel cell is equal to twice as much as the oxygen being consumed (every mole of oxygen reacted produces two moles of water). Percent error can then be determined to see if the water balance is verified.

Another value that can be calculated from the mass balance is the water ratio at both the anode and cathode. It is equal to the ratio of the partial pressure of water to the saturated pressure of water at the temperature of the humidifier, and can be calculated from the equation:

$$Water\ Ratio = \frac{\left(\frac{F_{H_2O\ vapor,out} + F_{H_2O\ liquid,out}}{F_{O_2,out} + F_{N_2,out} + F_{H_2O\ vapor,out} + F_{H_2O\ liquid,out}}\right)}{\exp\left(11.6703 - \frac{3816.44}{273.15 + T - 46.13}\right)} \quad (75)$$

Lastly, the water transport coefficient (α) can be determined, which is the ratio of the water flow exiting at the anode to the water produced in the fuel cell. Since the water produced is equal to twice the oxygen consumed, the water transport coefficient can be calculated from:

$$\alpha = \frac{F_{H_2O,out}^{A}}{2 \cdot F_{O_2,cons}} \quad (76)$$

4.0 Results and Discussion

The main objective of this project was to evaluate the operational data from PEM fuel cell at various stoichiometric feed coefficients and various diluted feeds of hydrogen. This section will introduce and discuss the collected data.

4.1 Stoichiometric Feed Variations: 1.5, 3 & 7.5

4.1.1 Impedance Spectroscopy

Impedance spectra were fit to a Nyquist curve using the process described in Galvanostatic Electrochemical Impedance Spectroscopy: Nyquist Fitting. For a stoichiometric feed, or λ, of 1.5, 3, or 7.5 the twelve Nyquist model parameters were optimized and are displayed in Table 4.

λ = 1.5				CATHODE					ANODE				
Experiment	Current (A)	L	Rohm	Rc (ohm)	Qc (F)	nc	Rd c (ohm)	Td c (s)	Ra (ohm)	Qa (F)	na	Rd a (ohm)	Td a (s)
220110C	3	2.00E-09	0.0044	0.0203	0.9502	0.9467	0.0066	1.4056	0.0018	1.4858	0.8000	0.0000	0.0000
210110K	6	3.30E-09	0.0045	0.0124	1.1191	0.9097	0.0039	0.6633	0.0013	1.3799	0.8000	0.0000	0.0000
210110N	9	3.30E-09	0.0044	0.0101	1.4845	0.8833	0.0043	0.5439	0.0010	1.6670	0.8000	0.0000	0.0000
λ = 3				CATHODE					ANODE				
Experiment	Current (A)	L	Rohm	Rc (ohm)	Qc (F)	nc	Rd c (ohm)	Td c (s)	Ra (ohm)	Qa (F)	na	Rd a (ohm)	Td a (s)
180110F	3	2.00E-09	0.0049	0.0199	0.9663	0.9270	0.0059	1.6114	0.0019	1.4914	0.8000	0.0000	0.0000
180110B	6	3.00E-09	0.0049	0.0122	1.0707	0.9097	0.0038	0.6871	0.0013	1.4014	0.8000	0.0000	0.0000
180110H	9	4.00E-09	0.0049	0.0099	1.3880	0.8731	0.0037	0.5233	0.0009	1.3734	0.8000	0.0000	0.0000
λ = 7.5				CATHODE					ANODE				
Experiment	Current (A)	L	Rohm	Rc (ohm)	Qc (F)	nc	Rd c (ohm)	Td c (s)	Ra (ohm)	Qa (F)	na	Rd a (ohm)	Td a (s)
210110C	3	4.00E-09	0.0055	0.0213	0.9025	0.9185	0.0066	1.3969	0.0020	1.2322	0.8000	0.0000	0.0000
210110F	6	4.00E-09	0.0061	0.0134	0.9550	0.8928	0.0038	0.7222	0.0014	1.1129	0.8000	0.0000	0.0000
210110H	9	4.00E-09	0.0063	0.0108	1.1231	0.8677	0.0031	0.4538	0.0010	1.1694	0.8000	0.0000	0.0000

Table 4: Stoichiometric Variation Fitting Results

R_{da} and T_{da} were assumed to be equal to zero because the hydrogen molecule is very small and there was very little water vapor and liquid on the anode side of the fuel cell. The anode diffusion resistance is taken at zero because the diffusivity of hydrogen was large enough to neglect the anode diffusion resistance and anode time constant.

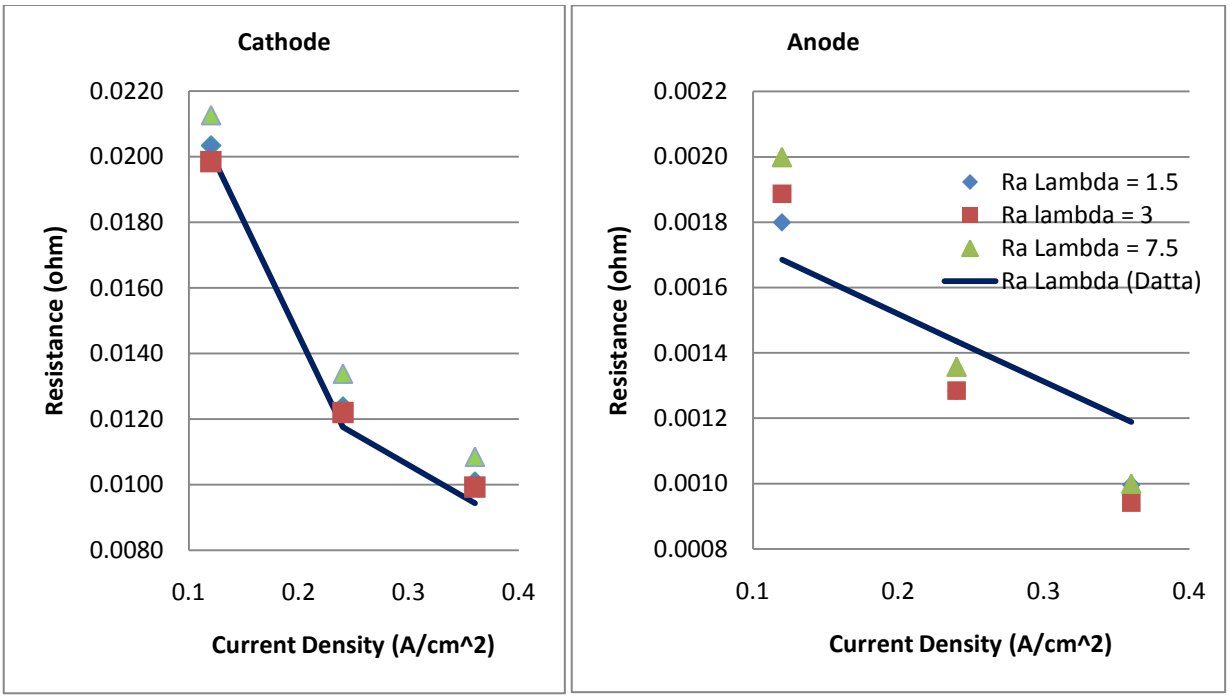

Figure 20: Charge Transfer Resistance in Stoichiometric Variations

Figure 20 shows that for an increased stoichiometric feed of 1.5, 3 and 7, the cathode charge transfer resistance decreases proportionally for each stoichiometric quantity as the current density increases. The greatest stoichiometric excess of 7.5 experiences a larger resistance than that of 3 or 1.5. Lambda 1.5 and 3 are too close to each other to clearly state which experiences a higher resistance. The anode charge transfer resistance exhibits similar behavior to that of the cathode, but the resistances are an order of magnitude smaller. This is because the hydrogen oxidation reaction which occurs in the anode occurs far more quickly than the oxygen reduction reaction in the cathode. The oxygen reduction reaction is slower because of the larger activation energy required for the oxygen reduction process than the activation energy required for hydrogen oxidation in the anode. The theoretical curves for cathode and anode charge transfer resistance do follow the trend for each value, and are closer to the values for 100 percent or Lambda 1.5 hydrogen flow than any of the stoichiometric cases.

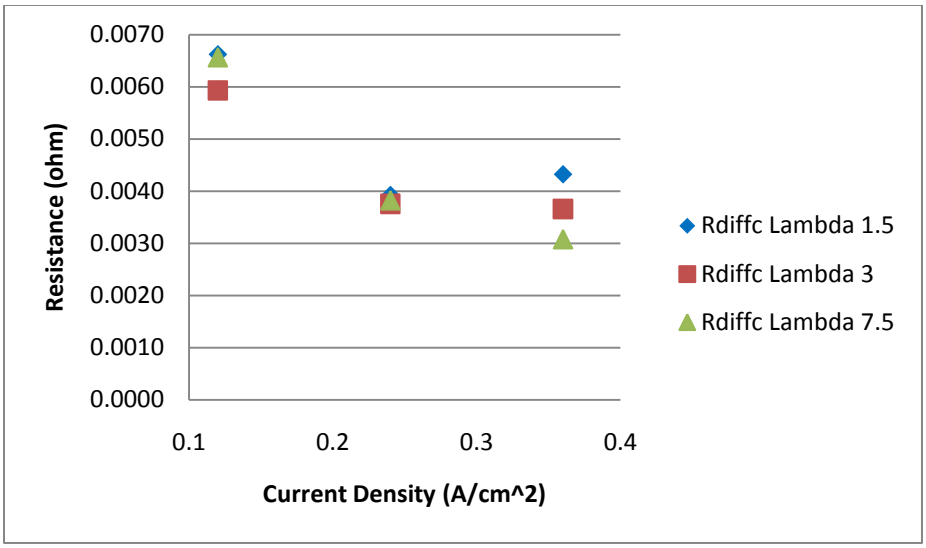

Figure 21: Cathode Diffusion Resistance in Stoichiometric Variations

The cathode diffusion resistance as shown in Figure 21 is higher at the lower current density. Unfortunately, our data did not provide very concrete results as to the relation between the stoichiometric feed amount and the diffusion resistance, except perhaps that the smallest stoichiometric feed rate experienced the highest diffusion resistance. For this experiment with pure hydrogen the anode diffusion resistance was assumed to be equal to zero because the hydrogen molecule is very small, thus the diffusivity of hydrogen is large enough to neglect the anode diffusion resistance.

4.1.2 Water Transport Coefficient

Figure 22 shows the water transport coefficient versus current density for the various hydrogen stoichiometric coefficient values.

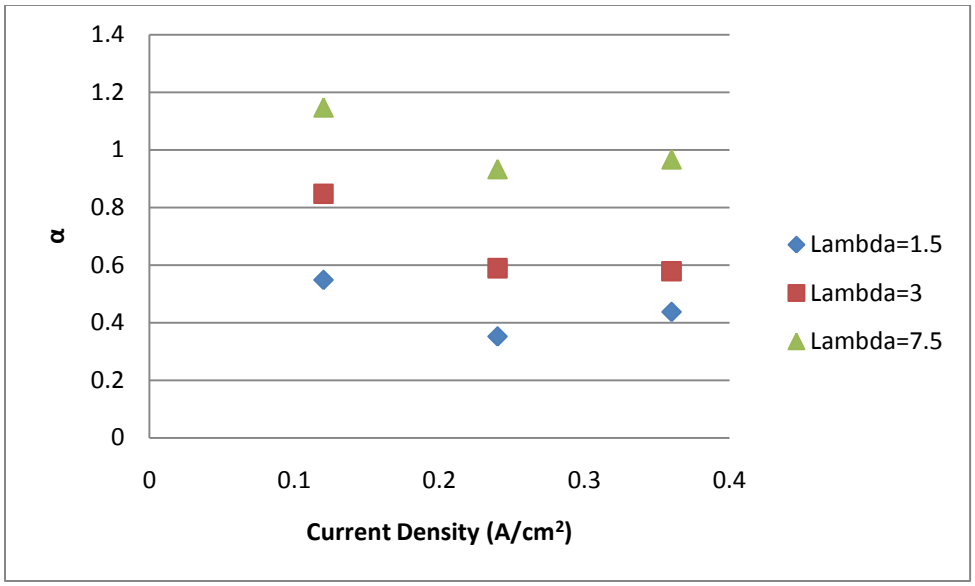

Figure 22: Water Transport Coefficients for Stoichiometric Ratio Variations

Since all of the calculated values for the water transport coefficient are greater than zero, this means that for all of these cases, the net flow of water goes from the cathode to the anode. In other words, since electro-osmosis results in water flowing from the anode to the cathode, the diffusion flux of the membrane is in the opposite direction, from the cathode to the anode, and is greater in magnitude. Also, as the stoichiometric coefficient increases, the water transport coefficient also increases, which means there is a greater net flow of water towards the anode.

4.1.3 Water Ratio

Figure 23 and Figure 24 show the water ratio at the anode and cathode for the various hydrogen stoichiometric coefficient values. The solid line at WR=1 signifies the point where there is saturated water vapor present at the fuel cell exit. Above this line, where the water ratio is greater than 1, there is liquid water present, and below this line, where the water ratio is less than 1, there is only water vapor present.

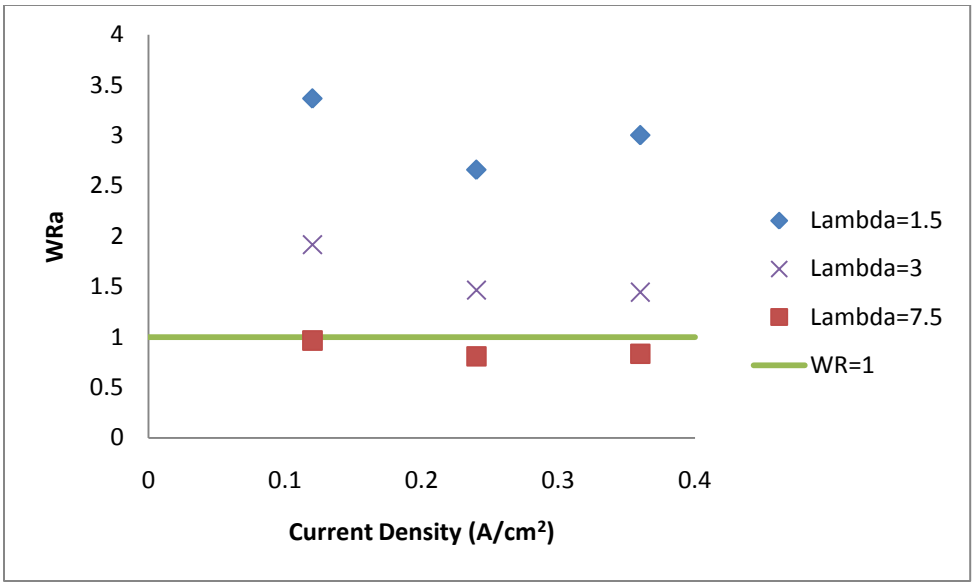

Figure 23: Water Ratio at the Anode for Stoichiometric Ratio Variations

From Figure 23, it can be seen that the water ratio is quite high at the anode for hydrogen stoichiometric coefficient values of 1.5 and 3, meaning that there is liquid water at the anode exit and therefore flooding exists inside the fuel cell. Raising the stoichiometric coefficient to 7.5 brings the water ratio below 1, which is to hinder flooding in the fuel cell.

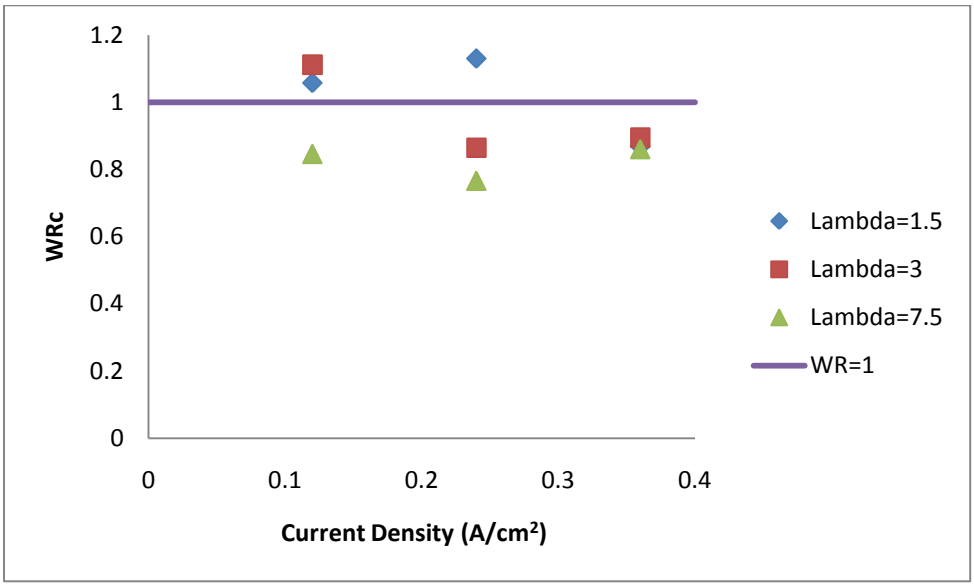

Figure 24: Water Ratio at the Cathode for Stoichiometric Ratio Variations

Figure 24 shows that at the cathode, there is liquid water present at low current density values. To eliminate the liquid water, the current density can be increased or the stoichiometric coefficient can be raised to 7.5.

4.1.4 Voltage

Figure 25 shows the voltage of the fuel cell versus current density for the various stoichiometric ratio values.

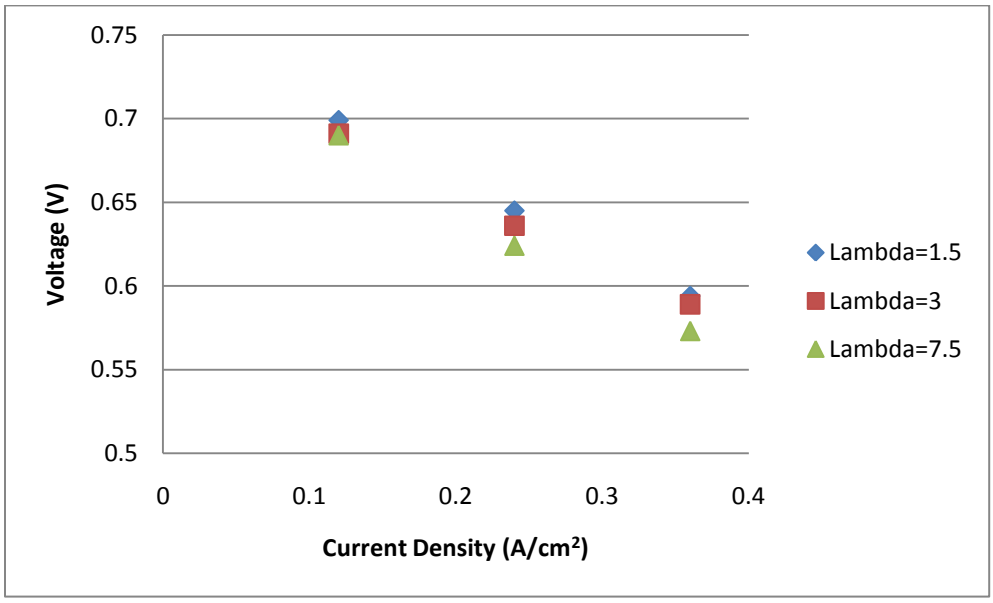

Figure 25: Fuel Cell Voltage for Stoichiometric Ratio Variations

The current density increases the voltage of the fuel cell decreases, which is expected due to activation losses, ohmic losses, and diffusion losses, as discussed in the section titled "Causes of Voltage Drop."

4.2 Hydrogen Feed Dilution: 10%, 20% & 50%

4.2.1 Impedance Spectroscopy

The second experiment performed in this project was the variation of the hydrogen feed concentration to the fuel cell at 10, 20 and 50 percent of the anode feed. We conducted

experiments at these conditions at 3, 6 and 9 Amps. The resulting data was modeled using the twelve Nyquist model parameters and is displayed in Table 5.

10%				CATHODE					ANODE				
Experiment	Current (A)	L	Rohm	Rc (ohm)	Qc (F)	nc	Rd c (ohm)	Td c (s)	Ra (ohm)	Qa (F)	na	Rd a (ohm)	Td a (s)
190110B	3	3.80E-09	0.0082	0.0213	0.7096	0.9219	0.0066	0.7778	0.0043	0.5826	0.8000	0.0098	0.7913
190110E	6	4.20E-09	0.0079	0.0134	0.7457	0.9042	0.0038	0.3311	0.0034	0.5570	0.8000	0.0075	0.3625
190110H	9	4.20E-09	0.0075	0.0108	0.7813	0.8785	0.0031	0.2345	0.0026	0.5540	0.8000	0.0094	0.2309
20%				CATHODE					ANODE				
Experiment	Current (A)	L	Rohm	Rc (ohm)	Qc (F)	nc	Rd c (ohm)	Td c (s)	Ra (ohm)	Qa (F)	na	Rd a (ohm)	Td a (s)
220110E	3	3.00E-09	0.0056	0.0212	0.9858	0.8802	0.0066	1.3511	0.0021	0.7814	0.8000	0.0101	1.4659
220110I	6	4.00E-09	0.0060	0.0134	0.9816	0.8751	0.0038	0.5733	0.0018	0.8077	0.8000	0.0040	0.5607
220110K	9	4.00E-09	0.0060	0.0112	1.1440	0.8493	0.0029	0.3784	0.0015	0.6971	0.8211	0.0037	0.3943
50%				CATHODE					ANODE				
Experiment	Current (A)	L	Rohm	Rc (ohm)	Qc (F)	nc	Rd c (ohm)	Td c (s)	Ra (ohm)	Qa (F)	na	Rd a (ohm)	Td a (s)
190110L	3	4.00E-09	0.0048	0.0199	1.0090	0.9211	0.0059	2.7503	0.0020	0.9289	0.8000	0.0115	2.9975
200110N	6	3.20E-09	0.0049	0.0122	1.0158	0.9244	0.0038	0.9812	0.0017	1.1170	0.8000	0.0042	0.9880
200110L	9	4.60E-09	0.0049	0.0100	1.2007	0.9007	0.0030	0.8263	0.0014	1.0100	0.8000	0.0061	0.8309

Table 5: Concentration Variation Fitting Results

The values for R_c, n_c, $R_{d,c}$ and n_a are fixed within 10% to the respective values found in the stoichiometric experiment with pure hydrogen. This was done to allow for the same more accurate fitting of the anode values. If some of the cathode values were not fixed, the excel solver function would be unable to solve for the anode values with any degree of certainty.

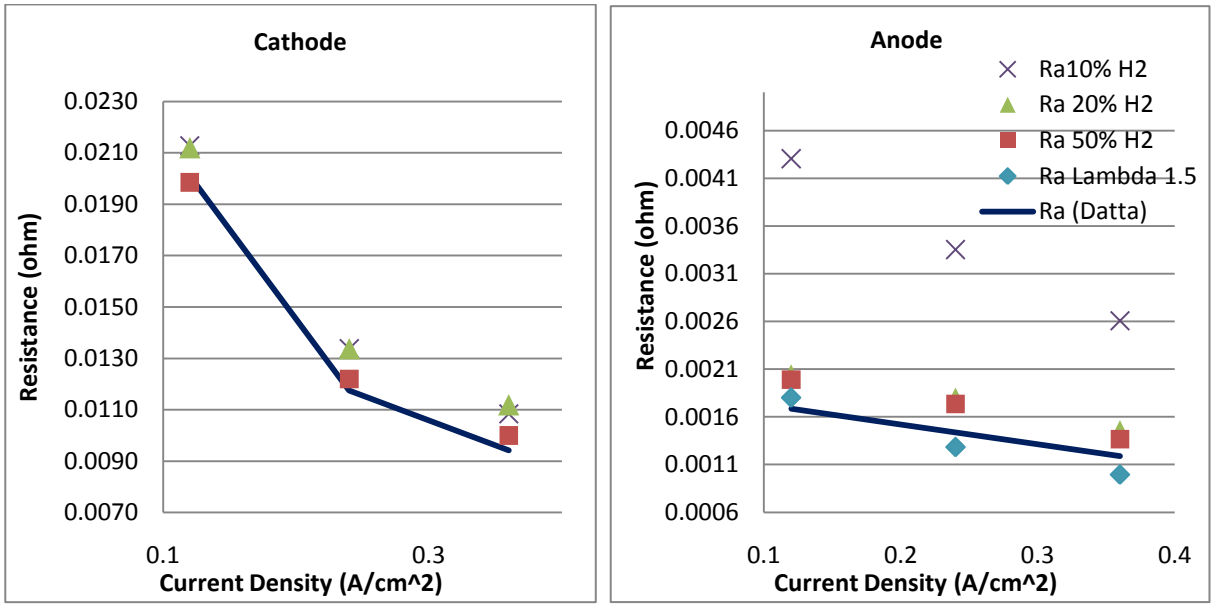

Figure 26: Charge Transfer Resistance Diluted with Hydrogen Feed

The anode charge transfer resistance for the case of a diluted hydrogen feed is shown in Figure 26. As expected, the resistance decreases as the current density increases. Also, the

highest resistance is exhibited by the least concentrated feed of hydrogen, and the lowest resistance is found when the feed consists of pure hydrogen. The theoretical curves for cathode and anode charge transfer resistance do follow the trend for each value, and are closer to the values for 100% hydrogen than any of the diluted cases. Thus the theoretical model is acceptable in its explanation of charge transfer resistances.

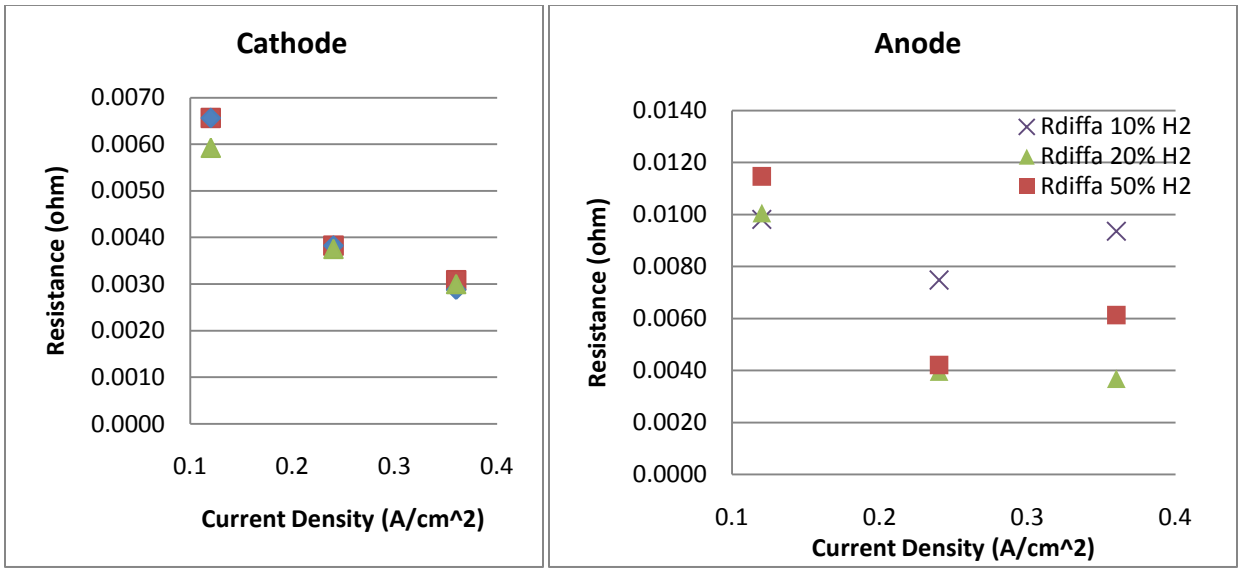

Figure 27: Diffusion Resistance Diluted Hydrogen Feed

As seen in Figure 27, the anode diffusion resistance in the case of 10% diluted hydrogen follows the theoretical curve of a slightly parabolic shape. PhD student Botao calculated the error values for the anode diffusion and charge transfer resistances using Matlab as we did not have the background in the program to allow us to do the calculation ourselves. The error in the experimental values collected for the anode diffusion resistance is very large. The error value for the charge transfer resistance value of the anode was larger than the value itself. The error value for the pseudo capacity of the anode was about 80%. These large error values are due in part to the fitting process and the fact that the anode diffusion loop is somewhat lumped in with the cathode diffusion loop. This data is similar to other experiments which have been conducted in the Nancy Laboratory.

As expected, the cathode diffusion resistance decreases as the current density increases. For the most part, the cathode diffusion resistance for each variation of diluted hydrogen feed is about the same. This is also expected because the proportion of gasses injected into the cathode remains the same regardless of how the hydrogen feed into the anode is varied.

4.2.2 Water Transport Coefficient

Figure 28 shows the water transport coefficient versus the current density for various concentrations of hydrogen gas. You can see that for pure hydrogen, the water transport coefficient is around 0.5, and the value increases as the concentration of hydrogen decreases. Concentrations of only 10% or 20% hydrogen in nitrogen have a water transport coefficient of about 1.

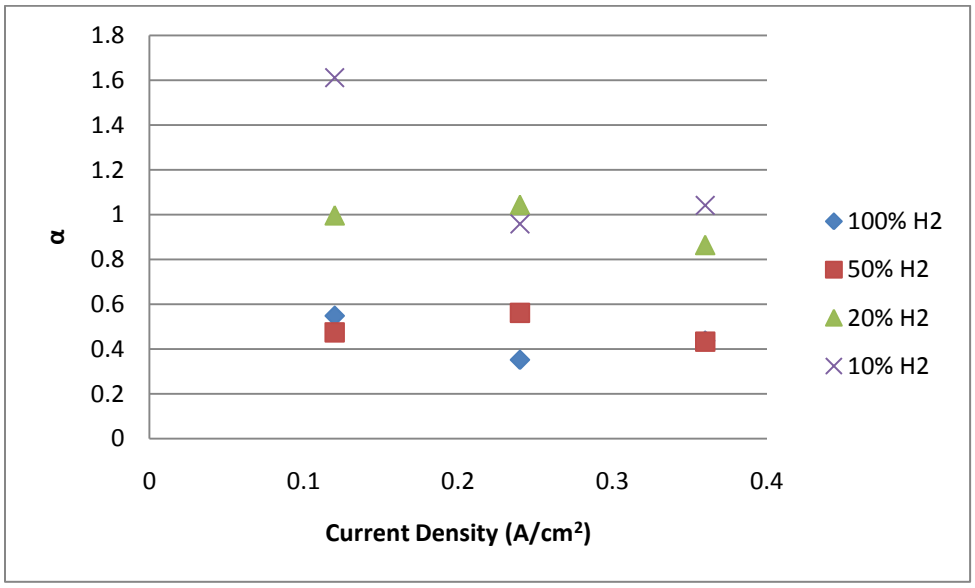

Figure 28: Water Transport Coefficient for Hydrogen Dilution Cases

The point at 0.12 A/cm^2 for 10% hydrogen is slightly unusual, and it can be attributed to an error in the water balance measurements. In measuring such small amounts of water, a small difference in mass can result in high error values. Also, the experiments for 3A were only done for 30-40 minutes to avoid damage to the fuel cell, so running them over a longer period of time might have resulted in different values.

Since all of the calculated values for the water transport coefficient are greater than zero, this means that for all of these cases, the net flow of water goes from the cathode to the anode. In other words, since electro-osmosis results in water flowing from the anode to the cathode, the diffusion flux of the membrane is in the opposite direction, from the cathode to the anode, and is greater in magnitude.

4.2.3 Water Ratio

Figure 29 shows the water ratio at the anode exit for various concentrations of hydrogen.

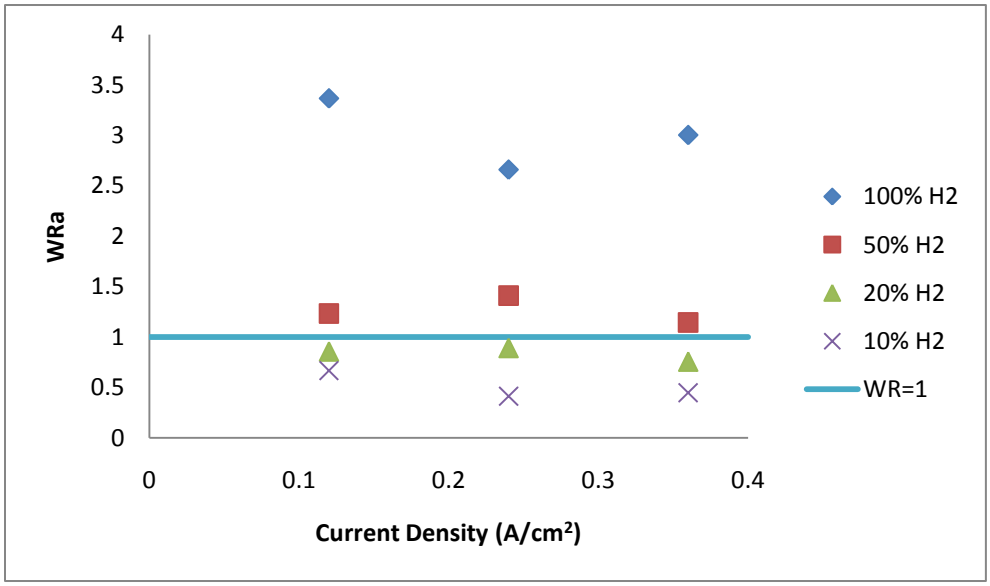

Figure 29: Water Ratio at the Anode for Hydrogen Dilution Cases

It can be seen that for 100% hydrogen, the water ratio is between 2.5 and 3.5, signifying a large amount of water at the anode exit. For 50% hydrogen, the water ratio is only slightly above 1, which means that there is flooding to a slight degree. For both 20% and 10% hydrogen, the water ratio is below 1, so there is no liquid water present at the anode exit.

Figure 30 shows the water ratio at the cathode exit.

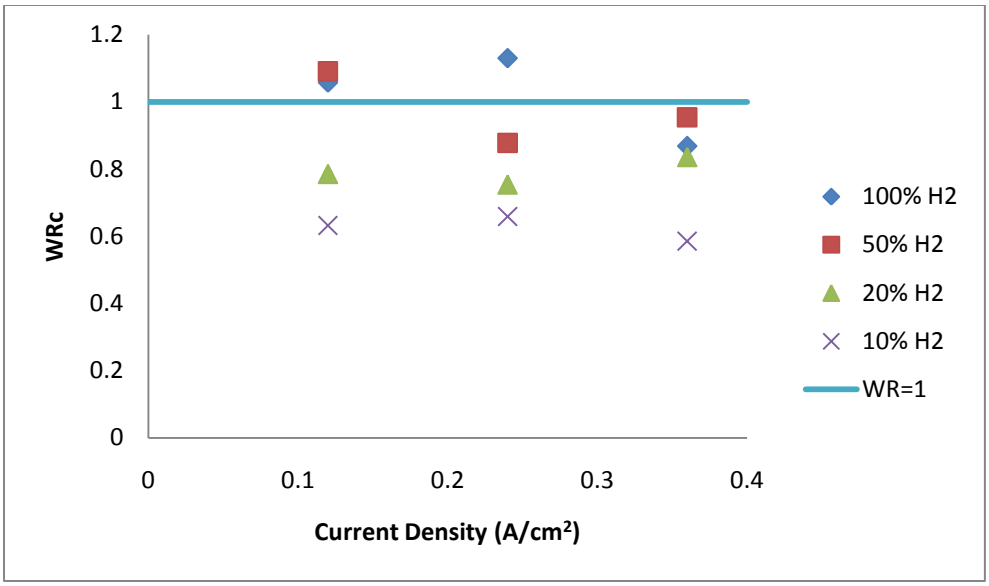

Figure 30: Water Ratio at the Cathode for Hydrogen Dilution Cases

At the lowest current density of 0.12 A/cm^2, there is liquid water present with both 100% and 50% hydrogen, but for higher values of current density and lower values of hydrogen concentration, there is only water vapor present at the cathode exit.

4.2.4 Voltage

In the case of 100% hydrogen the current density was varied between 0.12 and 0.64 A/cm^2. The resulting experimental current was graphed as a function of the current density and compared to the theoretical cell voltage; the calculations for this were explained in the Experimental Theoretical Cell Voltage section. The result can be seen in Figure 31.

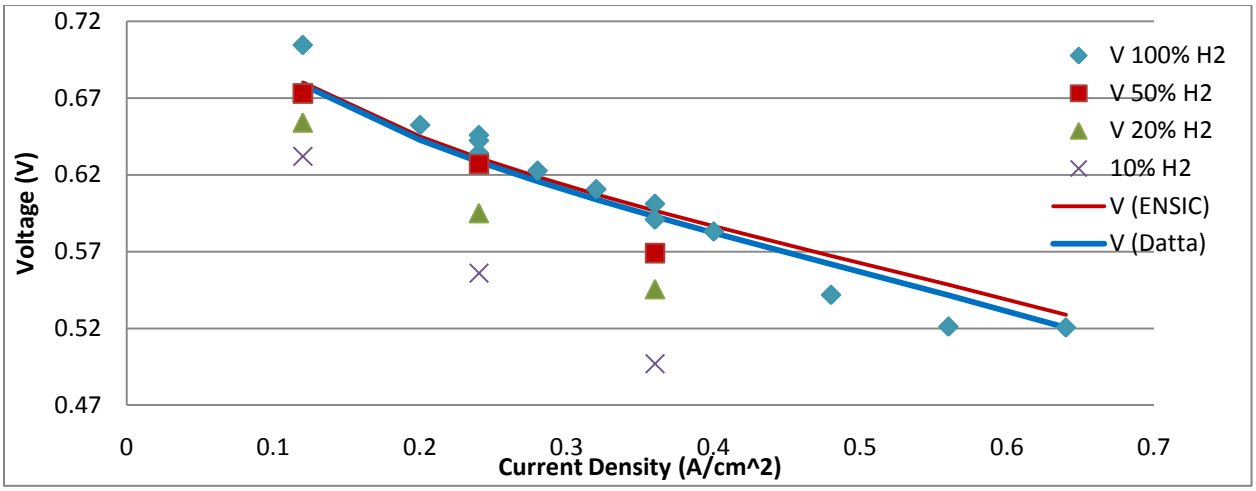

Figure 31: Cell Voltage Experimental and Theoretical

For the above cell voltage graph, the exchange current density for the cathode was calculated to be 8.9×10^{-6} A/cm^2. This value was confirmed by previous studies which have been conducted in the Nancy Laboratory. The values for $i_{0,a}$ and $i_{0,c}$ are of comparable magnitudes to published values of 0.087 and 0.035 mA/cm^2 (Tang, Lu and Liu, 2009). It should also be mentioned that $i_{0,a}$ is greater than $i_{0,c}$, a condition which is based on the electrochemical kinetics. Figure 34 also demonstrates that the theoretical models obtained both in Nancy France from ENSIC and from Ravindra Datta's class notes (Datta, 2010) predict similar voltages for given current densities.

4.3 Comparison

When looking at the fuel gas flow rates of the various experiments that were run, there are similarities between the dilution cases and the stoichiometric coefficient cases. Table 6 shows the flow rates in STP for the cases.

	3A	6A	9A
50% H_2	D_{H2}: 31.34 D_{N2}: 31.34 D_{Air}: 149.25	D_{H2}: 62.68 D_{N2}: 62.68 D_{Air}: 298.49	D_{H2}: 94.02 D_{N2}: 94.02 D_{Air}: 447.74
λ=3	D_{H2}: 62.68 D_{Air}: 149.25	D_{H2}: 125.37 D_{Air}: 298.49	D_{H2}: 118.04 D_{Air}: 447.74
20% H_2	D_{H2}: 31.34 D_{N2}: 125.37 D_{Air}: 149.25	D_{H2}: 62.68 D_{N2}: 250.73 D_{Air}: 298.49	D_{H2}: 94.02 D_{N2}: 376.10 D_{Air}: 447.74
λ=7.5	D_{H2}: 156.70 D_{Air}: 149.25	D_{H2}: 313.40 D_{Air}: 298.49	D_{H2}: 470.10 D_{Air}: 447.74

Table 6: Flow Rates for Experiments (in mL/min)

Since the 50% hydrogen cases have similar flow rates as the Lambda=3 cases, it would be expected that the results are similar. The same reasoning can be used with 20% hydrogen cases and Lambda=7.5 cases. Figure 32 through Figure 37 show the water transport coefficient and water ratio data for these experiments. They are indeed comparable.

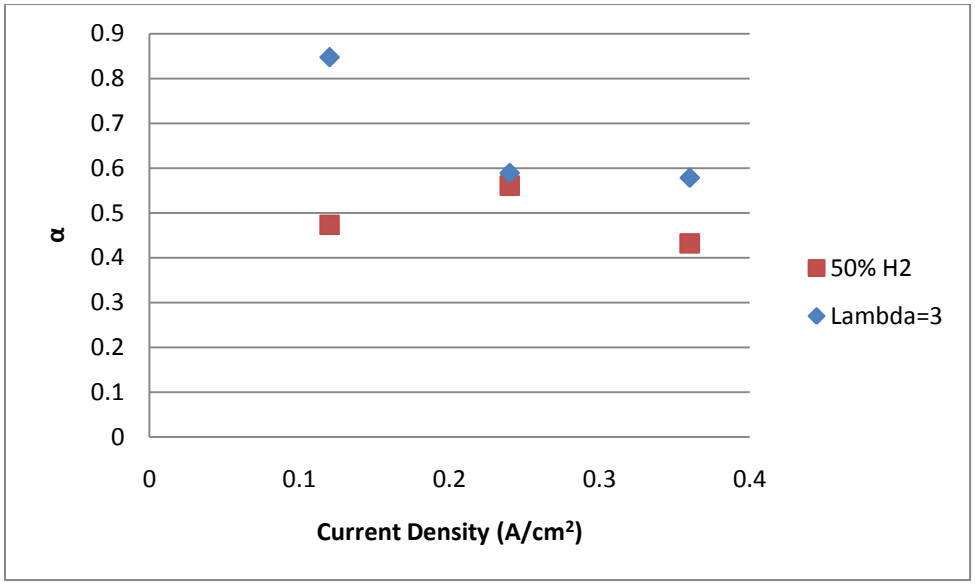

Figure 32: Water Transport Coefficient for 50% Hydrogen and Lambda=3

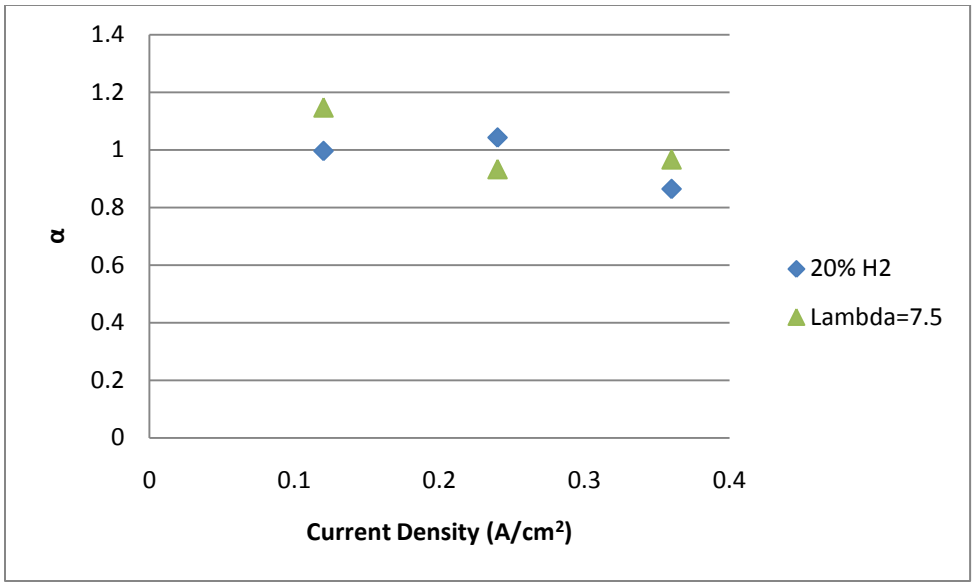

Figure 33: Water Transport Coefficient for 20% Hydrogen and Lambda=7.5

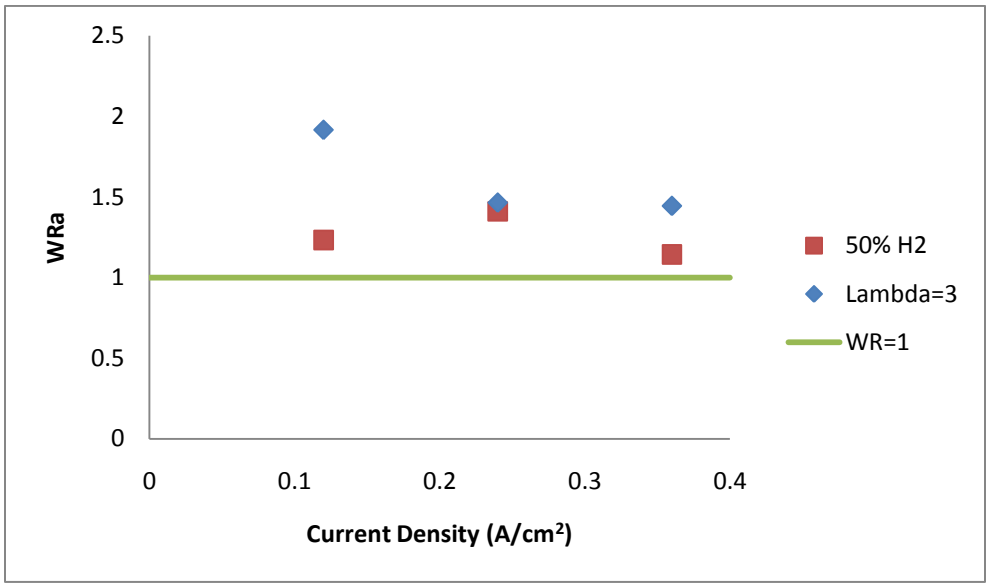

Figure 34: Water Ratio at the Anode for 50% Hydrogen and Lambda=3

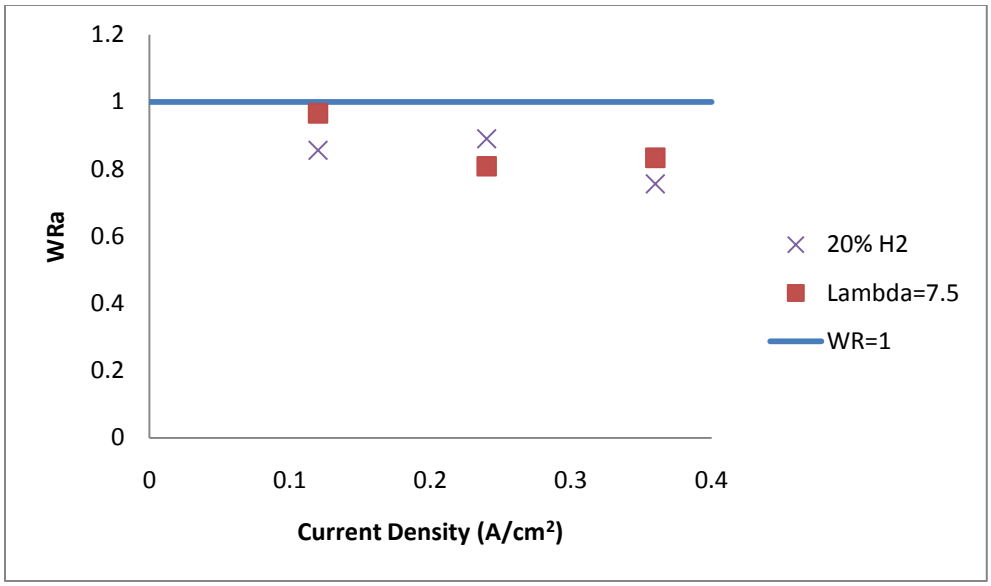

Figure 35: Water Ratio at the Anode for 20% Hydrogen and Lambda=7.5

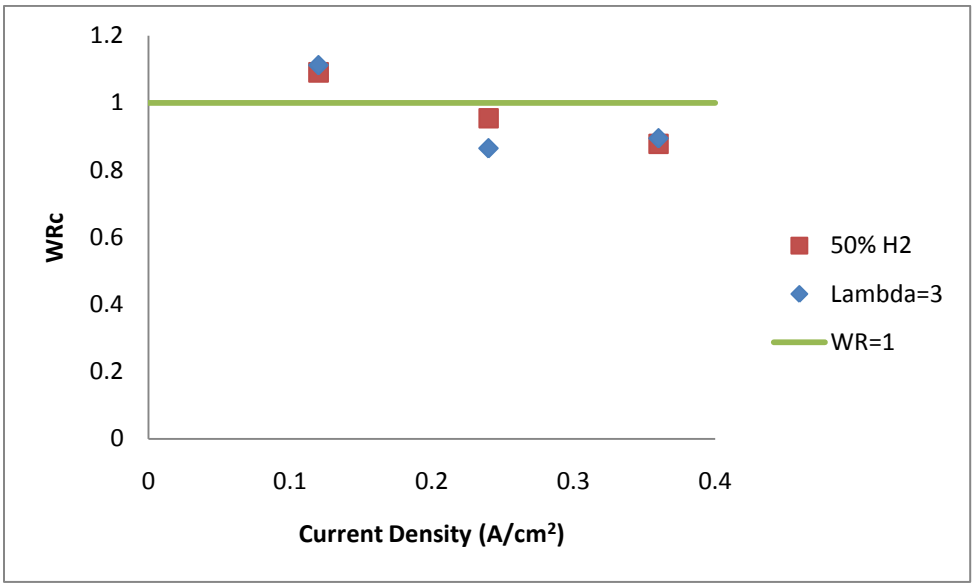

Figure 36: Water Ratio at the Cathode for 50% Hydrogen and Lambda=3

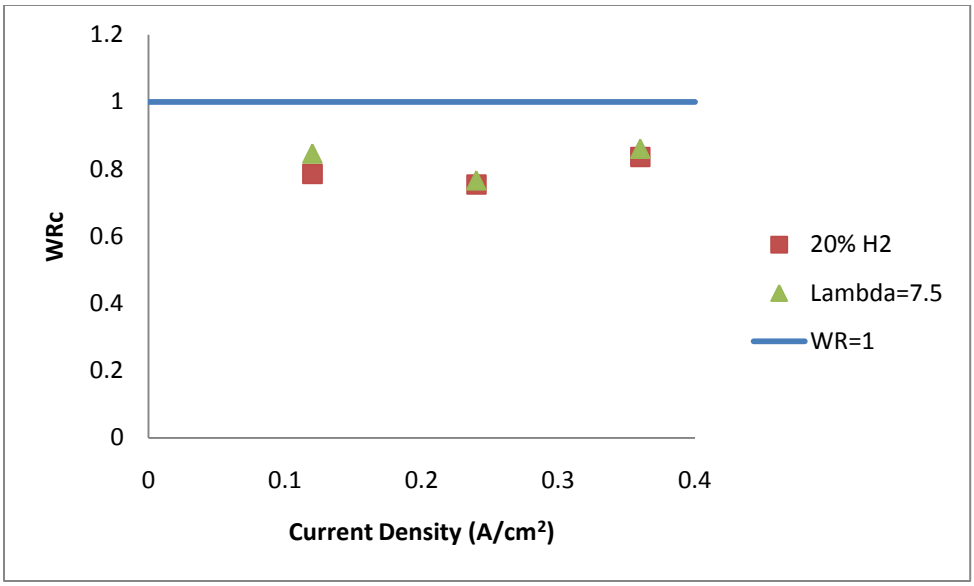

Figure 37: Water Ratio at the Cathode for 20% Hydrogen and Lambda=7.5

The exchange current density was calculated for 100, 50, and 20% hydrogen and the stoichiometric feed ratios of 1.5, 3 and 7.5 at currents of 3, 6, and 9 amps. The results are shown below in Figure 38 where the stoichiometric ratio values of 1.5, 3, and 7.5 correspond to hydrogen concentrations of 100, 50, and 20%.

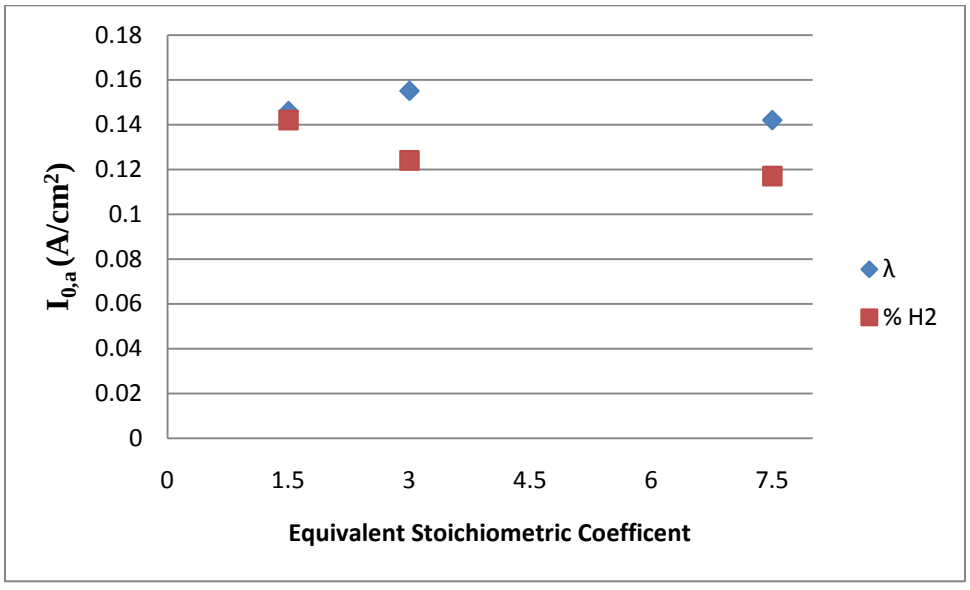

Figure 38: Exchange Current Density for Hydrogen Oxidation

It should be noted that $i_{0,a}$ does not vary largely with the stoichiometric coefficient. But in contrast, the anode exchange current density is a function of the partial pressure of hydrogen. As the partial pressure of hydrogen increases, so does $i_{0,a}$. This is because the exchange current density is proportional to the rate of reaction, and when hydrogen has a larger partial pressure, the reaction rate increases.

4.4 Open Circuit Voltage

Using Equation 10 for an operating temperature of 45.4°C, the theoretical OCV was found to be 1.2121 V. The actual OCV for the fuel cell was 1.1925, which is only a 1.6% difference and may be due to the interpolation of the Gibbs free energy value. Therefore, our theoretical equation for OCV models that of the actual fuel cell very accurately.

5.0 Conclusions and Future Work

From the impedance spectroscopy results, it can be seen that the ohmic resistance in the fuel cell remains constant regardless of the applied current density, but varies depending on the stoichiometric flow rate – where the $R_{ohm_{\lambda=1.5}} < R_{ohm_{\lambda=3}} < R_{ohm_{\lambda=7.5}}$. The charge transfer resistance of the cathode is an order of magnitude larger than that of the anode.

Charge transfer resistance decreases with increasingly pure hydrogen feed. The anode charge transfer resistance is difficult to determine since its value is obscured by the larger resistances of the cathode. Exchange current density for the cathode has been shown to increase as a function of increase hydrogen partial pressure. The exchange current density in the anode does not vary by a large degree. The variance may be accounted for by the reaction kinetics due to a decrease in temperature. In the case of 100% hydrogen, the cell voltage matched the theoretical voltage with a cathode exchange density five orders of magnitude smaller than the anode. Thus the anode exhibits a far better electron transfer rate. The cathode exhibits a smaller exchange current density and larger charge transfer resistance because the activation energy required for the oxygen reduction process in the cathode is much larger than the activation energy required for hydrogen oxidation in the anode.

Looking at the water transport coefficient, it can be determined that water is flowing in the direction of cathode to anode within the fuel cell. This is because the water is produced at the cathode, and there is also water fed to the cathode in the humidified air. The water ratio shows that 50% and 100% hydrogen cause flooding at the anode, unless the stoichiometric ratio is raised to 7.5. This is because having a higher stoichiometric ratio results in a higher flow of gas through the fuel cell, which dries out some of the water. At the cathode, raising the current density to 0.36 A/cm^2 eliminates liquid water at the exit for all concentrations and ratios. At lower current density values, there is liquid water present with 50% and 100% hydrogen. Again,

raising the stoichiometric ratio to 7.5 eliminates this liquid water. Lower hydrogen concentration reduces flooding because less water is produced in the overall reaction.

We are of the opinion that this project has fulfilled its objective of the characterization of a PEM hydrogen fuel cell as well as providing the Nancy University with data which may be used for further analysis of the behavior of fuel cells.

Bibliography

Barbir, Frano. PEM Fuel Cells: Theory and Practice. Ed. Elsevier Inc. Burlington: Elsevier Inc., 2005.

Bonnet, Caroline, et al. Electrochemical Investigation of The Effect of Carbon Monoxide On Platinum Anodes of PEMFC's. Laboratoire des Sciences du Genie Chimique, CNRS-Nancy Universite; Helion. Nancy, 2009.

Cahan, Dan, et al. History of Fuel Cells. 2006. 20 January 2010 <http://www.princeton.edu/~chm333/2002/spring/FuelCells/fuel_cells-history.shtml>.

Choi, Woojin, Jo W. Howze and Prasad Enjeti. "Development of an equivalent circuit model of a fuel cell to evaluate the effects of inverter ripple current." Journal of Power Sources (2006): 1324-1332.

Danzer, Michael A. and Hofer P. Eberhard. "Analysis of the electrochemical behaviour of polymer electrolyte fuel cells using simple impedance models." Journal of Power Sources (2009): 25-33.

Datta, Ravindra. "Introduction to Fuel Cells 2010." Class Notes, CHE 371X.

Dotelli, G., L. Omati and P. Gallo Stampino. "Influence of Carbon Cloth GDLs on Electrochemical Performance of PEMFCs." Proton Exchange Membrane Fuel Cells. Pennington: The Electrochemical Society, 2009. 1803-1810.

Fuel Cell. 5 January 2010. 21 January 2010 <http://en.wikipedia.org/wiki/Fuel_cell>.

Harper, Gavin D.J. Fuel Cell Projects For the Evil Genius. The McGraw-Hill Companies, Inc., 2008.

Lapicque, Francois. Investigation of Hydrogen Oxidation On The PEMFC Anode Surface: Effect of The Presence of Carbon Monoxide In The Hydrogen Stream And Reconciliation Of Two Models. Ecole Nationale Supérieure des Industries Chimiques, Institut National Polytechnique de Lorraine. Nancy, 2009.

Larminie, James and Andrew Dicks. Fuel Cell Systems Explained. West Sussex: John Wiley & Sons, 2003.

Matter, Paul H. Research. 28 January 2010 <http://www.chbmeng.ohio-state.edu/~matter/Research/Home_Open.htm>.

Nice, Karim and Jonathan Strickland. "How Fuel Cells Work." How Stuff Works. January 28 2010 <http://www.howstuffworks.com/fuel-efficiency/alternative-fuels/fuel-cell.htm>.

"Resin systems for advanced graphite composite fuel cell bipolar plates." Engineer Live. 28 January 2010 <http://www.engineerlive.com/Energy-Solutions/Power_Supplies/Resin_systems_for_advanced_graphite_composite_fuel_cell_bipolar_plates/21603/>.

Tang, Daoping, et al. "Calculations of the exchange current density for hydrogen electrode reactions: A short review and a new equation." Journal of Electroanalytical Chemistry (2009): Article in Press.

U.S. Department of Energy. Types of Fuel Cells. 23 June 2009. 19 March 2010 <http://www1.eere.energy.gov/hydrogenandfuelcells/fuelcells/fc_types.html>.